Bachelor Final Project
Degree in Chemical Engineering

Kinetic modelling of the dimethyl ether to olefins reaction over a HZSM-5 based catalyst

Simultaneous modelling of kinetics, deactivation and effect of water

Author:
Gontzal Lezcano

Directors:
Pedro Castaño
Tomás Cordero-Lanzac

Leioa, 22 June 2018

TABLE OF CONTENTS

1. INTRODUCTION

The development of new processes for producing light olefins from non-conventional and sustainable sources is a continuous and pressing target. Coherent with that premise arises a process that converts dimethyl ether (DME) into light olefins, also known as dimethyl ether to olefins (DTO), which has gained support.

1.1. LIGHT OLEFINS

Olefins or alkenes are unsaturated hydrocarbons that contain at least one double C=C bond, in which case are described by the C_nH_{2n} general formula. Particularly, light olefins (mainly ethylene and propylene) are high added-value products for the petrochemical industry (Weissermel and Arpe, 1981).

Ethylene (C_2H_4) is a colourless flammable gas with sweet odour and a boiling point of -104 ºC. From ethylene derive a plethora of products including polyethylene, polyvinyl chloride and polystyrene, which are essential for plastic and construction industries (Zimmermann and Walzl, 2012). Propylene (C_3H_6), which has a normal boiling point of -47 ºC, is also a building block in some remarkable processes, including production of rubber, polypropylene, acrylonitrile, propylene oxide and many others (Zimmermann, 2013).

In 2012 ethylene global production surpassed the barrier of 125 MMt, whereas the one of propylene reached 80 MMt (Hyde, 2012). Figure 1 depicts the sources of ethylene and propylene. As observed, ethylene is mainly produced through naphtha or light paraffin (predominantly ethane) steam cracking (Figure 1a). In the case of propylene production, steam cracking is also the predominant source, followed by FCC, being in both processes propylene a by-product (Figure 1b).
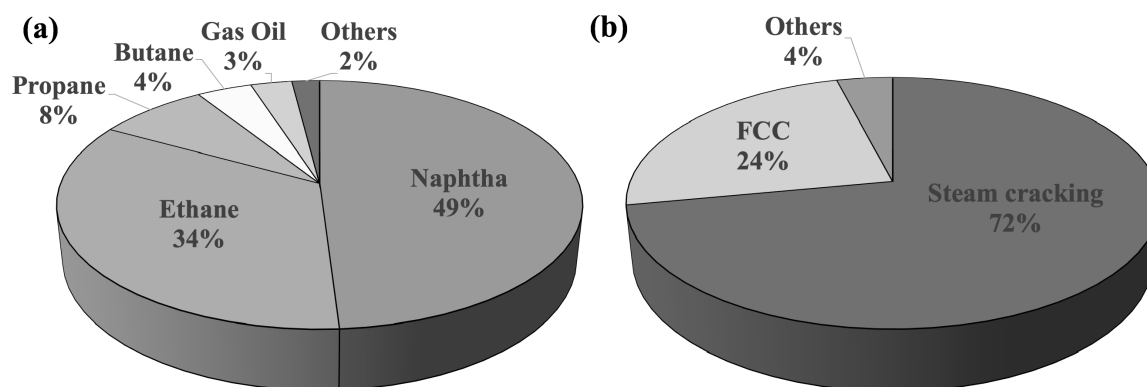
Figure 1. Global production of (a) ethylene by steam cracking feedstock and (b) propylene by process.

The nature of light olefin production relies on the context that surrounds it, yet generally speaking it can be defined as a flourishing industry. The availability of feedstock plays a paramount role in its development. For instance, a significant growth has been witnessed in both Middle East and Southeast Asia due to increase in feedstock availability in the area, ethane and naphtha for the steam crackers, respectively (Funk et al., 2013).

1.1.1. Steam cracking (SC)

Owing to all the evidences that have hitherto been mentioned, it remains clear that steam cracking is the chief source for light olefin production. It commonly uses a wide array of petroleum cuts as feedstock. The feedstock encompasses petroleum fractions of very diverse boiling range, including naphtha, kerosene, gasoil, way heavier hydrocracking residue or even lighter compounds like butane, propane or ethane. Besides, the latter virtually yields ethylene only, thereby being more selective towards the aimed products (Amghizar et al., 2017).

Steam cracking is a process from which key olefinic monomers (mostly ethylene, propylene and butenes) utilised in the petrochemical industry are obtained by means of thermal cracking of the hydrocarbon chains that comprise the feed. As a result, high purity olefins (>99 %) are obtained, as well as many other by-products such as H_2 (Lluch Urpí, 2011; Ren et al., 2006).

It is vital to evolve towards more sustainable processes for producing light olefins but developing a process which is also able to compete with the steam cracking seems to be a rather burdensome task. However, the increasing availability of crucial chemicals like methane or ethane plays a game-changing role. Prominent alternative technologies to steam cracking are presented in the adjacent Figure 2. These include catalytic dehydrogenation of alkanes (CDA), oxidative coupling of methane (OCM), Fischer-Tropsch synthesis (FTS) and methanol/DME to olefins (MTO/DTO) (Amghizar et al., 2017).
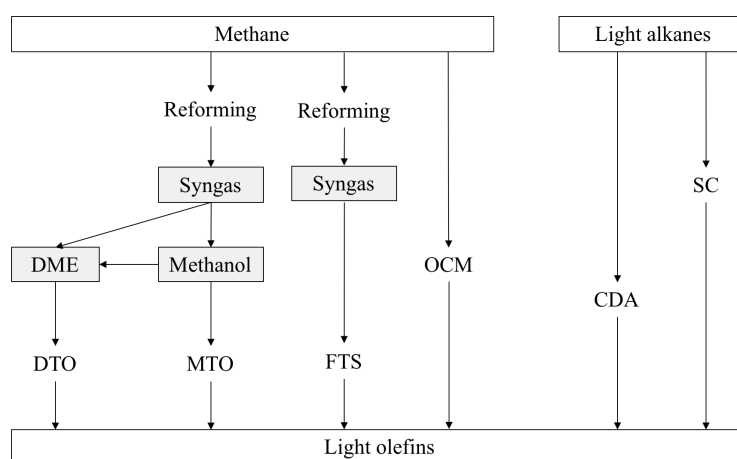
Figure 2. Current and pioneering technologies for producing light olefins.

1.1.2. Catalytic dehydrogenation of alkanes (CDA)

CDA is a catalytic process that entails dehydrogenation of light alkanes (ethane, propane, butane) employed as feedstock and yields the targeted light olefins. CDA reactions are accomplished with Pt-Sn or Cr_2O_3 catalysts, usually supported on alumina (Sattler et al., 2014).

It is a process that has already made the leap to industry, where *Oleflex* process by UOP is its main exponent. The core of the process is a fluidised bed, followed by a bunch of reactors in series, a product recovery section and a catalyst regeneration zone. The process is governed by an endothermic and equilibrium-limited reaction, hence high temperatures and low pressures are needed.

Its main advantage over steam cracking lies in the enhanced selectivity of a given olefin it reaps, which is strongly influenced by process operating conditions. Nevertheless, high operating

temperatures result in coke formation over the catalyst, being its regeneration problematic since the reversibility of the process is by far not complete. All in all, CDA is a quite mature technology that has a wide margin for improvement, especially in terms of reaction limiting equilibrium and energy efficiency.

1.1.3. Oxidative coupling of methane (OCM)

Technologies as yet explained (SC and CDA) mainly use light alkanes as feedstock. In OCM, on the contrary, methane shifts into ethane and ethylene straightforward by direct coupling of two methyl radicals in the gas phase (Olivos-Suarez et al., 2016),

The process directly turns raw material into ethane and ethylene, thereby removing inherent inefficiencies associated to other processes which convert the raw material to syngas as part of an intermediate process. On the other hand, drawbacks happen to outweigh advantages by cause of an immense reaction heat release and low conversions (about 20%) compared to other technologies due to abundant side reactions (Luo et al., 2013).

If the fact that this process was first reported in the early 80s is also mentioned, it can be concluded that OCM is still bereft of a robust understanding of its particularities that enables a short term industrial scale-up, and that more research is to be done therefore.

1.1.4. Fischer-Tropsch synthesis (FTS)

FTS is a technology that uses syngas as feedstock, catalytically transforming the syngas into a widely ranged (C_1-C_{100}) variety of products, including alkanes, olefins and oxygenates. Fe and Co are in the vanguard of FTS catalysis. FTS was first reported as a form of producing fuels out of coal in the 1920s, though its importance nowadays dwells in being a quite feasible source for producing light olefins form syngas, notably in countries lacking oil reserves, yet it is not as competitive as SC (Amghizar et al., 2017).

FTS typically shows limited selectivity of light olefins, which is to some extent explained by the diversity of products the process yields, as Schulz (1999) suggests, thus requiring higher product separation performances downstream reactor. So as to improve process performances, a better mechanistic understanding of the process urges.

1.1.5. Methanol to olefins (MTO)

MTO is a process in which light olefins are obtained from methanol, which commonly derives from syngas. Fed methanol abruptly swifts to a methanol, dimethyl ether (DME) and water equilibrium determined mixture (Menges and Kraushaar-Czarnetzki, 2012). Hence, MTO can be also accomplished by feeding DME, a process which is named DME to olefins (DTO) instead. Lurgi's methanol to propylene (MTP) is an example of the myriad variants MTO has (Khanmohammadi et al., 2016).

These are selective zeolite-catalysed processes. Even though reaction mechanisms in the past have long been discussed and not fathomed at all, the double cycle mechanism is gaining support as more and more authors are starting to converge on it (Amghizar et al., 2017). Furthermore, MTO has already found its niche in industry where UOP/Hydro MTO process stands out, using acid silicoaluminophosphate SAPO-34 as catalyst.

It consists of a fluidised bed reactor coupled to a regenerator, and coke deposited over SAPO-34 catalyst during the reaction is burnt therein, allowing a continuous reaction-

regeneration layout. Then, the effluent is cooled down so that the water it contains is removed from the resulting gaseous phase. The effluent stream is compressed and oxygenates are successively removed and recycled back to the reactor.

After the oxygenate recovery section, the effluent is further processed in the fractionation and purification section to remove contaminants and separate the key products (ethylene and propylene) from C_{4-6} ranged by-products (Funk et al., 2013). The C_4-C_6 fraction can be sent to the olefin cracking process (OCP) reactor where it is selectively converted to light olefins (the majority is propylene) and then further fractionated.
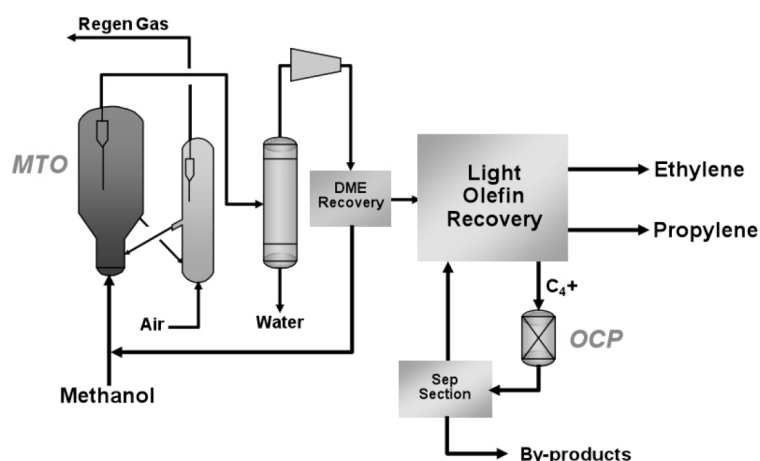

Figure 3. Scheme of UOP/Hydro MTO.

1.2. DIMETHYL ETHER TO OLEFINS

Because of the early 1970s oil shortages, the necessity of producing petrochemicals from oil free sources dawned. In this context, methanol to hydrocarbons (MTH) process by Mobil Research Laboratories (1976) is to be mentioned (Ilias and Bhan, 2013). This is based on a catalysed methanol conversion, reaping variable range hydrocarbons as a result. Catalysts are mostly made of zeolitic materials (Tian et al., 2015).

Initial reports indicated that light olefins could be obtained from the process, conforming the MTO, for light olefins (C_{2-4}) were abundant in test derived product spectra. However, Mobil researchers fortuitously detected that if reactions were not halted, greater ranged species including high olefins, paraffins, naphthenes and even aromatics could be produced starting from the lower olefins (Keil, 1999). In other words, the possibility to synthesise gasoline ranged hydrocarbons had been witnessed and the process was named methanol to gasoline (MTG). At this point, by the late 70s, New Zealand government decided to build pioneering facilities to produce gasoline from natural gas through methanol (Bjørgen et al., 2007).

It is worth mentioning that in every MTH process DME feed is also allowed due to rapid dehydration of methanol in contact with zeolite catalyst to form a methanol, DME and water mixture. Therefore, MTO and DTO happen to be analogue of one another reactionwise, sharing general reaction mechanism particularities. In terms of process operation, however, they are quite different, for methanol is handled as a liquid and DME is a gas when fed (Stöcker, 1999).

Much as oil price drops in the ensuing decades meant that MTH technologies were no longer profitable, the fact that oil-free petrochemical production is possible had been evidenced. Actually, today MTH processes are gaining strength and especially MTG, standing as a

promising alternative for gasoline access in an oil scarce or coal/natural gas/biomass plentiful future. More importantly, because both methanol and DME can be produced form renewable resources, MTO and DTO are deemed to be sustainable routes for obtaining light olefins, attracting special interest of researchers and industries as a result (Bjørgen et al., 2007).

In addition, in the case of MTO and DTO, they provide a wider and more flexible range of ethylene to propylene ratio than steam cracking to meet market demand, thus being even more noteworthy (Ghavipour et al., 2013).

1.2.1. Differences between DTO and MTO

Several major divergences do exist. First of all, the nature of the ways in which DME and methanol are obtained happen to be quite different. Methanol synthesis from syngas (STM) is conditioned by thermodynamic equilibrium, thus having a poorer per-pass and overall conversion, whereas DME produced through one step syngas to DME (STD) has no limitation whatsoever (Biryukova et al., 2011). In such way, better thermodynamics entail allowing bigger CO/H_2 ratios for DME synthesis, meaning that the use of DME as raw material in detriment to methanol has significant equipment and energy savings (Sardesai and Lee, 1998).

MTO standard catalyst is SAPO-34, which shows rather stable and selective performances. When reactions are triggered with DME, however, SAPO-34 tends to be rapidly hobbled by coke deactivation (Cai et al., 1995). That is the reason why ZSM-5 catalysts are preferred for DTO, which are more balanced in terms of deactivation, selectivity and activity. It is well-known that DTO leads to a more considerable deactivation by coke than MTO owing to the smaller amount of water present in the medium, which competes with coke precursors for adsorbing to catalyst sites, thus attenuating deactivation (Sardesai and Lee, 1998).

Al-Dughaither and De Lasa (2014) highlight that simple stoichiometric analyses depict a greater amount of hydrocarbons per unit mass of feedstock is obtained in DTO compared to MTO. They state if complete conversion is assumed, MTO yields 14 g of hydrocarbons per 32 g of feedstock, being the rest (18 g) the water formed within the process and thus 44 wt% of the feedstock turns into hydrocarbons:

$$CH_3OH = \left[CH_2 \right] + H_2O \tag{1}$$

where [CH2] is the average representation of the hydrocarbon product.

DTO, instead, produces 28 g of hydrocarbons and 18 g of water per mole of DME (46 g) fed, meaning that 61 wt% of the feed would become hydrocarbon products:

$$CH_3OCH_3 = \left[CH_2 \cdot CH \right]_2 + H_2O \tag{2}$$

where [CH2·CH2] is the average representation of the hydrocarbon product.

MTO suffers from slower reaction kinetics than the DTO, mainly because in the former there is more water in the reaction medium. Water attenuates the progress of all reactions, and in particular that of methanol dehydration. The attenuation takes place because water molecules adsorb to the catalyst acidic sites. The evolution with the time on stream (TOS) of hydrocarbon selectivity in both processes varies greatly from one catalyst to another, so that generic conclusions cannot be sketched in this regard (Gayubo et al., 2004).

A series of economic advantages could be reported in the DTO with respect to the water removal stage of the UOP/Hydro MTO process described in Figure 3, since less amount of water in the reaction medium implies a less exhaustive separation. The Following Table 1 summarises main benefits each process has with respect to the other.
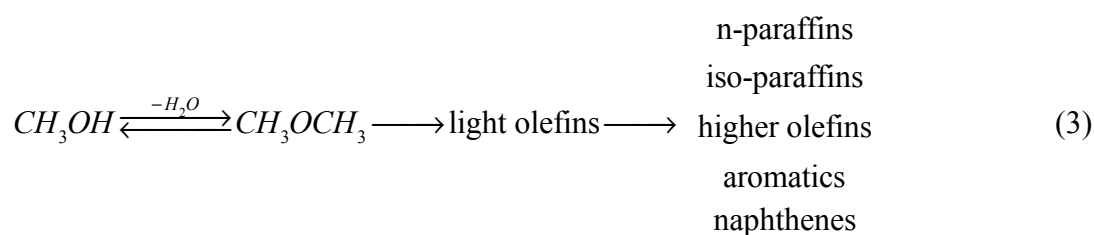
Table 1. Advantages of DTO and MTO by direct comparison.

DTO	MTO
✓ Thermodynamic, equipment and energy savings in producing the feedstock ✓ Greater amounts of hydrocarbons obtained per unit mass of feedstock ✓ Quicker reaction kinetics as there is less attenuation of the progress of the reactions by water ✓ Economic advantages due to a less exhaustive water removal stage being required	✓ Milder catalyst deactivation by coke due to a higher water deactivation attenuation

1.2.2. Reaction steps

DTO does not differ in excess from MTO provided that DME conversion into light olefins can also be regarded as a fundamental step within the MTO, methanol dehydration reaction rate is very high. Once the mixture composed of oxygenates and water in equilibrium determined concentrations is formed, light olefin formation reactions begin to appear.

The steady state production of higher olefins, naphthenes, aromatics and other hydrocarbons can be also attained, constituting the MTG, where previously formed lighter olefins undergo methylation, alkylation, oligomerisation, and more (Wang et al., 2015). It need not be said when aiming for lighter olefins letting reactions go this far yields undesired products. Overall MTG reaction scheme is as follows (Stöcker, 1999):

$$CH_3OH \underset{-H_2O}{\rightleftharpoons} CH_3OCH_3 \longrightarrow \text{light olefins} \longrightarrow \begin{array}{l} \text{n-paraffins} \\ \text{iso-paraffins} \\ \text{higher olefins} \\ \text{aromatics} \\ \text{naphthenes} \end{array} \qquad (3)$$

1.2.3. DTO mechanism

A general consensus is found in the literature for describing the methanol dehydration equilibrium (Ghavipour et al., 2013; Keil, 1999) and how it is attained (Lesthaeghe et al., 2006). Same does not apply for the formation of olefins, where C-C bonds are formed from oxygenates. In fact, 20+ mechanisms have been proposed so as to explain that phenomenon, early reports claiming C-C bonds and successive smaller olefins are conformed straightaway from DME and methanol.

Nonetheless, relevant evidences by Wang et al. (2003) suggest that a direct formation route from fed DME/methanol is prone to take place in the so-called induction period (non-steady

state) but not elsewhere, because if so, direct formation reaction rate would be neglectable and eclipsed even by impurities in the feed, catalyst or carrier gas (Song et al., 2002). Ilias and Bhan (2013) attribute it to the high existing activation energy barrier (~ 200 kJ mol^{-1}) to directly form the C=C bonds.

Alternatively, Chen and Reagan (1979) proposed that MTH mechanisms are explained by autocatalytic reactions. Coherent with that, Dessau and LaPierre (1982) stated that once olefins distinctive to the induction period are formed, they consecutively methylate to form higher olefins which also crack into lower olefins. This statement has been proven to be very insightful, for it incorporated a mechanism nowadays known as double-cycle. Anyway, these discoveries remained disregarded to a great extent (Sun et al., 2014).

Currently, literature agrees to adopt the hydrocarbon pool (HCP) as the more consistent theory to explain the reaction network. It was first drafted by Dahl and Kolboe (1993) and has continuously gained evidence, both theoretical and empirical, ever since. It is founded on the idea that a series of bigger molecules (referred to as a supramolecular inorganic–organic hybrid by X. Sun et al. (2014)) adsorb to catalyst cages, where methanol/DME are fed and light olefins and water formed. These reactions occur in a closed cycle, thus avoiding the formation of high energy level intermediates. In other words, HCP mechanism is often referred as the catalytic scaffold whose properties resemble those of coke and chemical formula is $(CH_m)_n$.

$$CH_3OH \: / \: CH_3OCH_3 \longrightarrow \left(CH_m\right)_n \longrightarrow \text{Light olefins} \qquad \text{where } 0 \leq m \leq 2 \qquad (4)$$

Identity and functioning of the HCP mechanism have been in detail defined for some specific catalyst systems. As an example, Arstad and Kolboe (2001) observed for SAPO-34 that HCP mechanism takes the form of highly methyl-substituted benzene rings, polymethylbenzenes, or the benzenium cations derived thereof. Same conclusions were drawn by Mikkelsen et al. (2000) for BEA and MOR. Anyhow, it is well known that HCP mechanism species varies with catalysts.

Besides, according to HCP mechanism theory, reactions taking part in the initial non-steady state induction period need not be same as those occurring in the steady state. As a result, HCP mechanism is inclusive with strong proofs witnessed under the direct formation theory (Lesthaeghe et al., 2006). In fact, whether species formed in the induction period affect HCP mechanism scaffold remains unproven, yet X. Sun and co-workers (2014) indicate so.

How HCP mechanism developed was still to be clarified. Before HCP mechanism was proposed in 1993, Tau et al. (1990) had already noticed that ethylene formation pathway might differ from the rest, thus not having a higher olefin parent. This concept opposed to the autocatalytic model, a benchmark back then, and went unnoticed. It was time after HCP mechanism theory had been reported, in 2006, when Svelle et al. (2006) presented the model today is more widely accepted, the double-cycle mechanism. The double-cycle mechanism is an evolved form of the HCP mechanism, which states that while ethylene is formed from (poly)methylbenzenes[1] in the so-called aromatics carbon pool (aromatic or arene cycle), the rest of olefins follow the olefin carbon pool (olefin or alkene cycle), where they derive from olefin methylation and interconversion (e.g. cracking). For this reason, the latter is also known as oligomerisation-cracking pathway (Tian et al., 2015).

---

[1] Poly written in brackets reflects that methylbenzenes vary with catalysts, from trimethylbenzenes to heptamethylbenzenes.

Reaction pathways are altered by pore architecture and acid strength of the catalyst. According to Ilias and Bhan (2013) the main overall steps of the double-cycle mechanism are the following, each being represented by single coloured arrows in Figure 4:

1. Olefin methylation: This is the step (blue arrows) by which the methyl groups from the dehydration of the feed ($CH_3OH \rightarrow H_2O + CH_2$) are incorporated into the pool. There are two proposed mechanisms for this step: one in which methanol and an olefin are adsorbed in a single acidic site and react in a single concerted stage, releasing water; another in which methanol dehydration occurs first to form a methoxide that is desorbed after reacting with an olefin.

2. Olefin cracking: This is what Dessau and LaPierre (1982) proposed, as previously mentioned (red arrows). If olefin cracking is considerably faster than the methylation of olefins, then the product distribution will be rich in light olefins. In other case, the product distribution will be rich in larger olefins.

3. Hydrogen transfer: The dehydration of methanol should lead to the formation of olefins $(CH_2)_n$; however, saturated alkanes and aromatic compounds are observed in the product distribution. The formation of alkanes requires new bonds to be added to chain, and that is balanced by the formation of hydrogen-deficient species, such as dienes, trienes, and (poly)methylbenzenes for MTH processes (green arrows).

4. Cyclisation: The olefin and aromatic cycles are related through stages of cyclisation and aromatic dealkylation. Cyclisation (purple arrow) is related to aromatisation provided that cycloalkanes and cycloalkenes are rapidly dehydrogenated to form aromatics.

   There are two possible routes for cyclisation and aromatisation of olefins. One involves the dehydrogenation of olefins to form dienes and trienes which are cyclised to aromatics. In the second route, olefins first form cycloalkanes and subsequently dehydrogenate to form aromatics. In both routes, dehydrogenation occurs through hydrogen transfer reactions in which olefins or cycloalkanes donate hydrogen to other hydrocarbons that act as hydrogen receptors.

5. Aromatic methylation: Aromatics, specifically (poly)methylbenzenes, play a crucial role in MTH process since these species, together with olefins, act as scaffolds for methylation. Same two mechanisms explained in the olefin methylation stage apply to the aromatic methylation (orange arrows).

6. Dealkylation of aromatics: In this step (pink arrows), light olefins and ethylene (separately) are formed almost exclusively through dealkylation of aromatics. This permits the linkage of both cycles or carbon pools again and thus tailor the closed double-cycle.
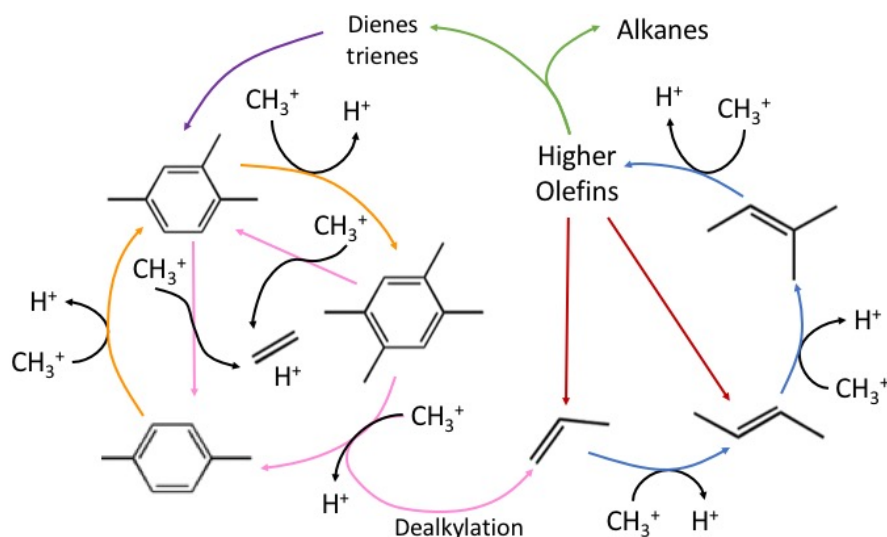
Figure 4. Double-cycle mechanism general steps.

1.2.4. Catalysts

DTO catalysts are predominantly zeolites or zeolite-like.

Today, SAPO-34 is the most widely used catalyst in MTO industrial processes, a silicoaluminophosphate, although many others have been studied over time, like SAPO-5, SAPO-17 or SAPO-18 (Chen et al., 1994). For DTO purposes, however, they are not suitable for different reasons: fast deactivation (SAPO-17 and SAPO-34), low performance (SAPO-5) or not having required activity (SAPO-18) (Aguayo et al., 2005; Wendelbo et al., 1996).

Catalysts of larger cavities than SAPOs have also attracted researching interest, among which BETA, IM-5, TNU-9 or Y zeolites are noteworthy (Bleken et al., 2011). These allow relatively large species (penta, hexa-methylbenzenes) to be part of the HCP mechanism scaffold, originating many different products, favouring the methyl-aromatic and polyaromatic products, and hence low selectivity of olefins. Besides, the nature of the products formed favours the formation of coke.

Facing the challenge of having a good selectivity and a slow deactivation, ZSM catalysts of an intermediate pore size (lower than the catalysts exposed so far) peak (Chen et al., 1999). ZSM-22, for instance, inhibits the HCP arene cycle, thus yielding aromatic-free products since methylation and cracking pathways prevail. However, the outcoming C_5+ rich product spectrum is an undesirable selectivity of light olefins indicator (Teketel et al., 2010). ZSM-11, on the other hand, shows good resistance to deactivation, but Derouane and co-workers (1981) claim its selectivity is substantially lower than that of ZSM-5, archetype of DTO/MTO catalyst. In fact, Harrison et al. (1987) observed more than twice as much trimethyl benzene in ZSM-11 than in ZSM-5, where toluene and xylenes predominate.

By and large, ZSM-5 is one of the catalysts that best compensates the activity and selectivity with stability. Indeed, Al-Dughaither and De Lasa (2014) determined, , that a very acidic ZSM-5 (Si/Al=15) with respect to a less acidic (Si/ Al=40) and a seldom acidic (Si/Al=140) has higher activity at both zero time and TOS. Higher acidity makes the effect of temperature on deactivation also more pronounced. That is why it is important to know how a ZSM-5 with high acidity deactivates when performing DTO/MTO reactions, as it could lead to the

development of a catalyst for DTO/MTO with good selectivity (better than BETA or Y) and good stability (better than SAPO-18 or SAPO-34) (Pérez-Uriarte et al., 2017).

Zeolites

Zeolites are microporous crystalline aluminosilicates. Their framework is composed of series of tetrahedra of Si or Al bonded to one another by commonly shared oxygen atoms. Every tetrahedron consists of a Si or Al atom placed in its core and oxygen atoms in each of the four vertexes constituting the tetrahedron. When tetrahedra bond to one another by the oxygen atoms, units are built and channels, channel intersections and voids of pores in form of cages emanate (Flanigen, 1991).

Si tetrahedra are neutral in terms of electric charge. When the Si atom is replaced by an Al atom, a negatively charged tetrahedron results, because a 4^+ charged atom has been substituted for a 3^+ atom (Jha and Singh, 2016). So as to overcome positive charge insufficiency the presence of extraframework inorganic and organic cations is justified, which form spacious pores or rings. Zeolite pore channels are microscopically small, hence their other name - 'molecular sieves', where water molecules are also spotted. As a result, zeolite chemical formula is the following (Weitkamp, 2000):

$$A_{y/m}^{m+}\left[\left(SiO_2\right)_x\left(AlO_2^-\right)_y\right]zH_2O \tag{5}$$

where A is the extraframework cation with m^+ charge, x+y is the number of tetrahedra per crystallographic unit, x/y is the proportion of Si and Al in the structure, known as Si/Al ratio.

Si/Al ratio dwindles between a host of values, being 1 the minimum value suggested by Loewenstein (1954), who reported that finding two adjacent AlO_4^- tetrahedra stood little chance because of the electrostatic forces exerted by the negative charged nature of them and being infinite the maximum representing the entirely siliceous form which are polymorphs of SiO_2.

Other elements like B, Zn or P can also be conjoined to the framework, giving an array of different groups. One is the aluminophosphate group, formed by neutral and non-acidic structures born from the alternation of AlO_2^- and PO_2^+ within the structure. On the other hand, whenever regular Al atoms in silicoaluminates are replaced by P atoms, silicoaluminophosphates (SAPO) type frameworks arise. Further research on how distinct groups can be spotted by addition of metallic cations is being done (Cheetham et al., 1999).

Zeolites can be natural or synthetic, although synthetic ones are in vogue. These tend to result in a more uniform and purer state as compared to the natural types in terms of their lattice structures, sizes of pores and cages in their frameworks. Features of the zeolites formed strongly depend on the synthesis temperature and pressure, concentration of the reagent solutions, pH, process of activation and aging period and SiO_2/Al_2O_3 content of the raw materials (Jha and Singh, 2016). If classified according to their Si/Al (Payra and Dutta, 2003):

1. Low Si/Al (1-2) ratio: Its major exponents are zeolites A and X. Having a high cation content and thus favouring their exchange, these zeolites have been studied and implemented since their discovery in 1959.

2. Intermediate Si/Al (2-5) ratio: Its greatest exponent is the Y zeolite, fundamental in catalytic processes with hydrocarbons such as the FCC catalyst. Despite having a

structure similar to that of X, for having less Al shows greater thermal stability and acidity.

3. High Si/Al (10-100) ratio: Its greatest exponent is the ZSM-5, with ratios between 10 and 100. They are characterized by having an adequate acidity for catalytic reactions involving hydrocarbons, despite their low Al content.

Generally speaking, as Si/Al ratio is increased, properties such as acid resistivity, thermal stability or hydrophobicity are boosted, unlike acidic site density or cation concentration, which drop (Jha and Singh, 2016).

<u>Catalyst guideline</u>

Catalyst appropriateness is built upon three limitations: activity, selectivity and deactivation.

Catalyst activity is closely related to deactivation, as well as to temperature. Typically, activity increases as working temperature rises, but so does coke deactivation, which plummets catalyst activity over time. It can also be stated that activity is positively influenced by the acidity of the catalyst, which increases as the Si/Al ratio decreases, owing to Al atoms being capable of creating strong acidic sites in the catalyst structure. However, acidity also stimulates coke formation, speeding up the deactivation (Al-Dughaither and De Lasa, 2014).

Selectivity is primarily affected by catalyst pore size, because the more sizeable the channel intersection is, the bigger HCP scaffold species are, and therefore, a more diverse spectrum of products is obtained (shape selectivity). A wide spectrum of products involves no other but smaller selectivity of a particular olefin, as repeatedly explained in the literature (Bjørgen et al., 2009). Quoting Teketel and co-workers (2010), that happens 'due to the steric limitation imposed by the relatively narrow pores'. In addition, other variables such as cage size (Svelle et al., 2007), acidic site concentration or operating conditions also influence the selectivity, which decreases as the deactivation progresses (Chen et al., 1994).

Deactivation, as in any other catalytic process, arises due to deposition of carbonaceous material (coke) that is adsorbed on the Brønsted and Lewis sites of the catalyst, thus blocking the pores. More specifically, as suggested by Müller et al. (2015), the deactivation process has two entirely differentiated parts: one in which intraporous coke acidic site blocking at channel intersection is witnessed, and another in which outer blocking of zeolite channels is sighted.

Anyway, deactivation is a function of both zeolite pore structure and operating conditions. The type of zeolite completely conditions deactivation, since the latter strongly relies on characteristics such as geometry and crystal size, strength of acidic sites or concentration of acidic sites. For example, it is well known that the higher the concentration of acidic sites, the greater the deactivation rate, although its effect is less than that of the crystal geometry. On the other hand, it is known that condensation reactions predominate at low temperatures; at higher temperatures, hydrogen transfer reactions top (Müller et al., 2015).

1.3. KINETIC MODELLING

In order to enable a wider industrial scale-up of DTO processes, better kinetic and catalyst deactivation knowledge is needed, for they are key in reactor design. One of the most interesting procedures of acquiring that knowledge relies on modelling the kinetics of the process involved. When catalytic processes kinetics modelling is concerned, regular kinetic modelling implies an

immense amount of rate coefficients. These are dependent on reactive and product species configuration (Froment, 2005). With the purpose of tackling the problem, single event kinetic and lumping models are mainly employed by researchers.

Single event kinetic models are based on molecular level analyses, which enable deducing kinetic equations for reactions between different molecules. Lumping models, on the contrary, are the outcome of a macromolecular scale study in which compounds taking part are grouped into lumps according to their properties (e.g. boiling point, solubility, etc.) to then state the governing kinetic equations (Becker et al., 2016).

It is sensible to think that lumping modelling is accurate when macroscopic effluent characteristics are targeted, as well as not requiring an exhaustive feed examination. Single event kinetic modelling, however, has the potential of reporting information not accessible when lumping modelling such as describing reactivity of each component at a fundamental level or optimising product distribution (Cordero-Lanzac et al., 2018). Yet, they are also computationally more complex than lumping models, which have little need of thermodynamic considerations and describe catalyst deactivation more easily. Thereby, the use of lumping models is more extended and usually preferred in industry (Sabbe et al., 2011).

When lumping modelling is concerned, the number of lumps present in the model is variable. The choice of lumps is always a compromise between the capabilities of the analytical techniques to characterise and quantify them on one hand, and the needs of the final user in terms of model prediction and precision on the other. In most cases, the analytical techniques are the limiting step and force the choice of the lumps. Over time, thanks to the development of the available computing power, lumped models have become more and more complex with a continuous increase in the number of lumps (De Oliveira et al., 2016). For example, for modelling the fluid catalytic cracking, Weekman and Nace (1970) proposed a 3-lump based model back in 1970; by 1999, a 18-lump model already existed (Pitault et al., 1994), and today models with approximately 3000 lumps exist (Christensen et al., 1999). Figure 5 shows the 3-lumped and 18-lumped models.
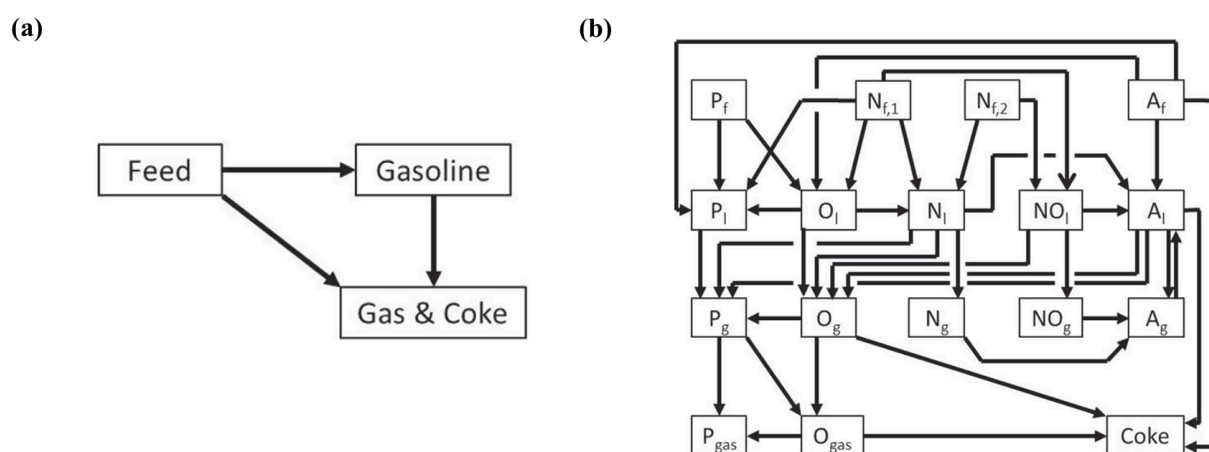
Figure 5. Illustration of the evolution of the lumped kinetic models for the catalytic cracking process: (a) Weekman and Nace (1970) and (b) Pitault et al. (1994).

Lumped kinetic models are relatively easy to develop because the number of lumps and the number of reactions remain limited. Moreover, due to the multi-compound characteristics of the lumps, the reaction pathways are generally global, and their rate equations are often simple (e.g. elemental reaction orders). In other words, their main advantage is their simplicity. Their

kinetic parameters are often determined by minimising the deviations between model and experimental data (De Oliveira et al., 2016).

In the literature, scarce research has been done about kinetic modelling of ZSM-5 catalysts with DTO purposes, let alone a model with a deactivation equation too. Pérez-Uriarte and co-workers (2017) proposed a kinetic model for the transformation of DME into olefins, considering catalyst (low acidic ZSM-5) deactivation. The scope of this work is to propose a 9-lump kinetic model for DME transformation into olefins over a very acidic (Si/Al=15) ZSM-5 catalyst, considering its deactivation. The proposed mathematical methodology enables calculating the kinetic parameters for each step of the reaction scheme and catalyst deactivation kinetics by means of fitting the experimental data of evolution with time on stream of the lump concentrations. Different kinetic equations describing catalyst deactivation established for the MTO process have been used as a basis to find the most suitable one for describing the corresponding to the DTO process.

2. OBJECTIVES

This Bachelor Thesis is focused on the simultaneous kinetic modelling of the catalytic transformation of dimethyl ether into light olefins and catalyst deactivation. The catalyst employed is a very acidic HZSM-5 (Si/Al=15), knowing that this catalyst is stable and faces a potential industrial scale application. For the fulfilment of these objectives, the following milestones are proposed:

- Evaluate the real performance of the catalyst proposed for the DTO reaction in different operation conditions and confirm whether the results obtained are coherent with the studies reported in the literature.

- Analyse the impact of a stronger water presence in the reaction medium (by co-feeding it) in the main reaction indexes (conversion and selectivity) and in the catalyst deactivation.

- State different kinetic models for the DTO reaction and for the used catalyst that are capable of predicting the experimental results obtained with a pure DME feed at both zero time and time on stream.

- Select the model that shows a better fitting by statistical discrimination, as long as the selected model has a reasonable physical meaning.

- Contrast the validity of the model chosen when water (with DME) is also fed into the reactor.

3. MATERIALS AND METHODS

3.1. CATALYST PREPARATION

The targeted catalyst to be prepared and employed is 50 wt% HZSM-5 active phase, 30 wt% pseudoboehmite support and 20 wt% α-alumina promoter.

With such purpose, 18.5 cm^3 colloidal dispersion of α-alumina (Alfa Aesar, 20 wt% Al_2O_3), which is the promoter or inert filler, were poured into a vessel. While being stirred at constant pace, 9.09 g of pseudoboehmite (Sasol Germany, 70 wt% Al_2O_3) binder or support were gradually added. At the same time, deionised water was also being poured so as to ensure homogeneity of the mixture in the vessel. Then, 10g of Zeolyst International supplied HZSM-5 (Si/Al=15) active phase were supplemented.

Pseudoboehmite binder is fundamental, for its presence derives in a mesoporous matrix of γ-Al_2O_3 during the calcination step. Besides, the agglomeration with pseudoboehmite as a binder enhances the mechanical resistance of particles and provides particles with meso- and macropores, easing its use (Cordero-Lanzac et al., 2018). Still, pressure drop across the fixed bed constituting the reactor is not considerable and is maintained within reasonable values. Note that pressure drop is one of the most important process variables that needs to be controlled when fixed bed reactors are concerned.

Because of the characteristic hydrophilicity of the active phase, catalyst samples were dried before being weighed. Once the samples had been mixed for 3 h, catalyst particles were obtained by means of wet extrusion. Resulting extrudates were dried at room temperature for the following 12 h, and afterwards, dried for 12 h more in a furnace at 100 °C. Once completely dried, catalyst sieving was performed so that only particles of suitable diameter size for the fixed bed reactor (between 0.125 mm and 0.300 mm) remained (Pérez-Uriarte et al., 2016b).

Lastly, catalyst particles were calcined in a muffle furnace to obtain the acidic and hydrothermally stable zeolite-based catalyst. In order to make calcination possible, previously the catalyst needed to be heated up at a constant pace (5 °C min^{-1}) for 2 h. Once required temperature reached, catalyst underwent calcination at 575 °C for 2 h. In detail, calcination is founded on a controlled dehydroxylation of the strongest Brønsted sites that enables recovery of kinetic properties of the catalyst even after successive regenerations by coke oxidation. Once calcinated, samples were left for cooling in the oven for 2 h.

As a result of the thermal treatment, pseudoboehmite conversion to a γ-Al_2O_3 matrix of middle acidity was accomplished. That provides the catalyst with a hierarchical mesoporous structure, in which the microporous crystals of the zeolite are embedded. Furthermore, those mesopores in the matrix inhibit blockage of micropore mouths of the HZSM-5 crystals by external coke (Guisnet et al., 2009).

3.2. CATALYST CHARACTERISATION

Whenever lab-scale catalytic tests are performed, it is essential to be aware of its physical and chemical characteristics. Indeed, knowing textural and acidic properties of the catalyst employed was targeted.

3.2.1. Adsorption-Desorption of N_2

Quantification of the surface area of the catalyst is considered to be fundamental and that was done by N_2 adsorption-desorption. It consists of the physical adsorption of nitrogen in a catalyst sample by putting them in contact.

This technique made possible determining the following structural features of the catalyst:

a) BET surface area (S_{BET}). S_{BET} was determined by the Brunauer-Emmet-Teller method which is a fairly common method used for determining surface area, despite its theoretical limitations. The physisorption isotherm was converted into the ''BET plot'' and from it the specific surface area could be calculated.

b) Mesopore surface area (S_{mes}) and micropore volume ($V_{micropore}$). Both were determined by the t-method, in which a t-curve of a reference compound (similar to the sample) was compared to the t-curve of the sample itself. Harkins-Jura was the t equation used.

c) Mesopore volume ($V_{mesopore}$). $V_{mesopore}$ was computed by subtracting micropore volume to the total pore volume. The total pore volume is calculated from the maximum value of N_2 adsorbed, generally at the partial pressure of 0.995.

The technique was executed in a Micrometrics ASAP 2010 at -196 ºC. With such purpose, firstly samples were degassed at 150 ºC for 8 h so that impurities were removed. Then, samples were weighed, and mass losses noted down. ASAP 2010 works by adding nitrogen, measuring and storing the amount of adsorbed gas volume in the sample. It continuously repeats the nitrogen addition, waiting, measuring and storing process until the required nitrogen partial pressure range (from 0.01 to 1 at -196 ºC) in order to obtain the isotherm has been fulfilled.

Table 2 shows the main textural parameters obtained for the catalyst. As it can be seen, the catalyst exhibits a specific surface area of 285 m² g⁻¹ and a predominantly mesoporous porous texture ($S_{mesopore} = 131$ m² g⁻¹, $V_{mesopore} = 0.393$ cm³ g⁻¹).

Table 2. Pysicho-chemical properties of the catalyst.

Property	Value
N_2 adsorption-desorption	
S_{BET} (m² g$_{cat}$⁻¹)	285
$S_{mesopore}$ (m² g$_{cat}$⁻¹)	131
$V_{micropore}$ (cm³ g$_{cat}$⁻¹)	0.065
$V_{mesopore}$ (cm³ g$_{cat}$⁻¹)	0.393
NH_3 temperature programmed desorption	
Total acidity (mmol NH_3 g$_{cat}$⁻¹)	0.41
Average acid strength (kJ mol⁻¹)	115
h-peak (ºC)	325
t-BA temperature programmed desorption	
Total acidity (mmol t-BA g$_{cat}$⁻¹)	0.47
Average acid strength (kJ mol⁻¹)	120
l-peak (ºC)	205

3.2.2. Temperature programmed desorption of NH_3 and t-BA

Catalyst acidity was characterised by temperature programmed desorption (TPD). It consists of handling the required energy to desorb a base probe that has been previously chemisorbed in a catalyst sample. Probe weight loss during TPD experiments is usually plotted using the derivative curve against temperature in the so-called TPD profiles or thermograms.

In the lab TPD was performed for two base probes (NH3 and t-BA) with a Setaram DSC-11 calorimeter connected to an injection Harvard pump that enables heat flux and adsorbed mass variations measurements at the same time. The equipment is completed by online coupling to a mass spectrometer (Thermostar, Balzers Instruments) programmed to measure desorbed base probe. As a result, catalyst acidity is determined by mass of base probe chemisorbed per unit mass of catalyst.

First of all, sample was swept with He at a flow rate of 60 cm^3 min^{-1} at 550 ºC for 30 minutes to remove impurities. Afterwards, process was stabilised with a 20 cm^3 min^{-1} flow rate of He at 150 ºC and 100 ºC for NH_3 and t-BA respectively. Once stable, at the same temperature, sample saturation was attained by continuous addition (via injection) of the corresponding base probe (50 μL min^{-1} for NH_3 and 10 μL min^{-1} for t-BA). The base probe saturated sample was then swept again with 20 cm^3 min^{-1} of He aiming to remove to all the physisorbed probe. Finally, TPD was performed at 550 ºC for ammonia and 500 ºC for t-BA by raising temperature at a constant heating rate of 5 ºC min^{-1}.

Nature of acidic sites and amount of acidic sites (total acidity) were determined by peak analysis and mass of probe per unit mass of catalyst (mmol NH_3 g_{cat}^{-1} and mmol t-Ba g_{cat}^{-1}), respectively. In fact, the total acidity was calculated from the area under the TPD profile, whereas the average acid strength was given by the calorimeter and corresponds to the heat of probe desorption.

During the TPD experiment, desorbed probe was being measured through the mass spectrometer. Desorbed ammonia was detected at a signal of m/z=15, whereas a signal of m/z=56 corresponded to butene (main products of t-BA cracking). For this reason, the criterion for associating the registered peaks of TPD profiles with the strength of acidic sites (nature) is different in each case. In the case of NH_3, l-peak represents the amount of weak acidic sites in the catalyst while h-peak represent stronger ones, for in the case of that probe, desorption of weak and strong sites occurs at lower and higher temperatures, respectively. Opposite criterion applies to t-BA.

The calculated total acidity of the catalyst (Table 2) is similar in both methods (0.41 mmol NH_3 g^{-1} and 0.47 mmol t-BA g^{-1}). Since NH_3-TPD and t-BA-TPD allow determining the total amount of acidic sites and the ones capable of cracking t-BA, respectively, an efficient activity of the acidic sites is suggested. Likewise, the average acid strength calculated from NH_3 adsorption-desorption is comparable to that obtained from t-BA experiment, as depicted in Table 2. Both results also point out the predominant presence of strong acidic sites, as contrasted in Figures 6a and 6b. Figure 6a portrays the 325 ºC peak (h-peak) observed in the NH_3-TPD profile, whereas Figure 6b shows the l-peak in the t-BA-TPD profile, at 205 ºC. Note that reporting high acidity sites is consistent with the low Si/Al molar ratio of the zeolite.
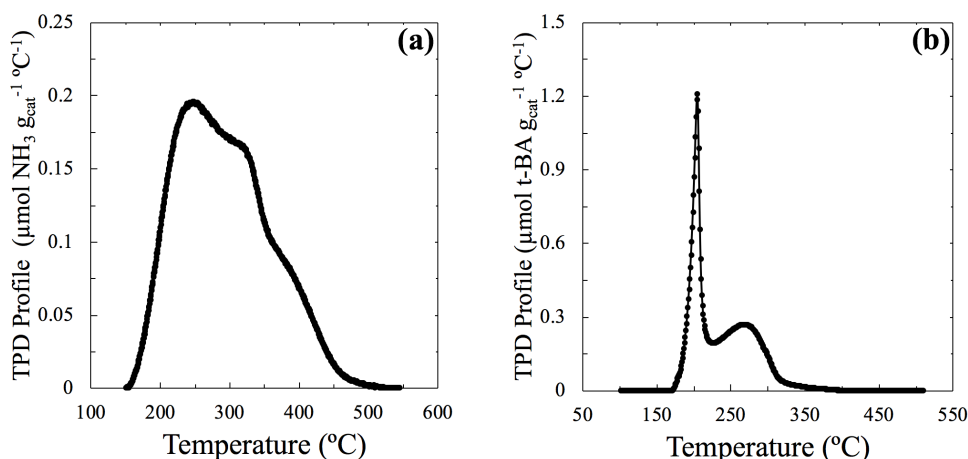
Figure 6. Determination of the presence of strong acidic sites, by h-peak and l-peak detection in NH_3 and t-BA TPD profiles, respectively.

3.3. REACTION EQUIPMENT

Reactions have been accomplished in a Microactivity Reference by PID Eng. & Tech. (Madrid, Spain) automatic reaction equipment, shown in Figure 7. As it can be seen, a fixed bed reactor and a micro-gas chromatograph (μ-GC) are its principal components.
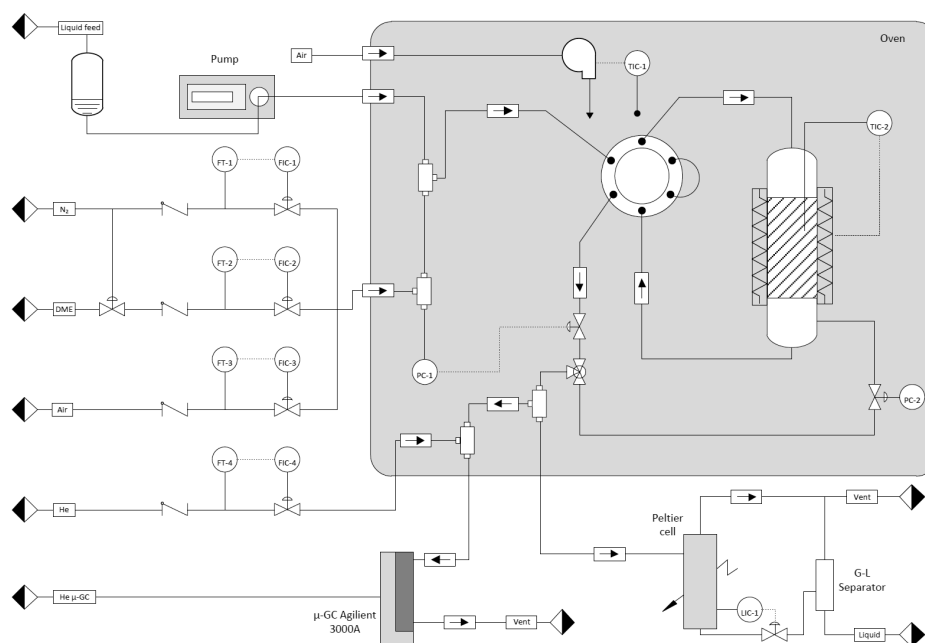
Figure 7. Scheme of the Microactivity Reference (PID Eng. & Tech.) automatic reaction equipment used.

N_2, He, DME and air are the gases used for the experiments. Gases were fed from storage vessels to the system through flow rate controllers, which are Bronkhorst High Tech. B.V. Series, right after flowing past a check valve that blocks backflow. In case DME/water co-feeding was necessary, liquid water was pumped using a HPLC pump and then mixed with the DME flowing just before being introduced in the oven (Figure 7).

After entering the oven, a 6-port pneumatic valve permitted the feed to either bypass the reactor to the chromatograph or flow across the reactor. The former configuration was used for feed analysis. If the gaseous mixture was taken to the reactor, reactions were accomplished as the mixture flowed through the bed.

Lastly, a small fraction of reaction products (1 cm^3 sample) was diluted with He (flow rate of 40 cm^3 min^{-1}) before being analysed and concentration determined in the micro-gas chromatograph. The remainder products were taken to the Peltier cell and cooled down to 0 ºC and condensates (at 0 ºC, 1.5 bar) were afterwards separated in the gas-liquid separator from the lighter non-condensable compounds. The latter were vented to the atmosphere.

3.3.1. Reactor

The reactor used is a 9.1 mm inner diameter 316 stainless-steel down-flow reactor by Autoclave Engineers. Notwithstanding the 305 mm total length of it, only 100 mm comprise the effective bed length it provides. The reactor is contained inside a cylindrical stainless-steel reaction chamber and heated by a ceramic-coated electrical resistance, when necessary. Such chamber is placed inside the oven.

100 mm effective reactor length is not attained by just filling the corresponding amount of catalyst. Instead, the bed is completed with carborundum (VWR Chemicals) SiC inert material (0.5 mm<d_p<0.6 mm) homogeneously mixed with the catalyst and quartz wool (Panreac Química) placed in both ends of the bed.

3.3.2. Experimental runs

It is noteworthy mentioning that prior to each run, DME transformation (unlike the methanol transformation) required a conditioning treatment of the catalyst in situ (at 550 ºC with air for 2 h) to remove the water adsorbed on the acidic sites of the catalyst. The experimental operating conditions for obtaining light olefins from DME were: 325–375 °C, 1.4 bar, space time up to 2 g_{cat} h mol_C^{-1} and time on stream (TOS) up to 15 h. Same set of experiments were performed for a pure DME feed and a DME/water mixture feed (H_2O/C molar ratio of 1).

3.3.3. Chromatograph

The chromatograph used is an Agilent 3000A μ-GC with 4 analytic modules that permitted determining product concentration every 8 minutes (duration of the analytical method). Feed used during the process was analysed with it as well. Each module has a fixed injector, a TCD detector and a separation column, and thereby, each module is able to separate certain compounds. Columns in the μ-GC are: molecular sieve (MS-5) in which H_2, CO and CH_4 are identified; Parapak Q (PPQ) in which CO_2, H_2O and DME are identified; alumina in which ethane, ethylene, propane, propylene, iso-butane, n-butane, trans-2-butene, 1-butene, iso-butene, cis-butene, iso-pentane, n-pentane, cyclo-pentane and pentenes are identified and Stabilwax in which methanol, hexanes, heptanes, benzene, toluene and xylenes are identified.

Due to the large number of components present in the reaction, the composition of the product stream were grouped into the following lumps: (i) olefins; (ii) paraffins; (iii) BTX; (iv) C_{5+} and; (v) CO_x. Each one of these lumps are respectively composed of: (i) ethylene, propylene and butenes (iso-butene, 1-butene, trans-2-butene and cis-2-butene); (ii) ethane, propane and butanes (iso-butane and n-butane); (iii) benzene, toluene and xylenes (o-, m- and p-xylene); (iv)

iso-pentane, hexanes and heptanes and; (v) CO and CO_2. Other single-compound lumps were also included: CH_4, methanol, DME and H_2O.

3.4. REACTION INDEXES

In order to analyse the experimental results obtained, the following indexes were defined:

Conversion: It was defined as the reacted (F_C-F_D-F_M) carbon molar flow rate per unit reactor inlet (total) carbon molar flow rate.

$$X = \frac{F_C - F_D - F_M}{F_C} \tag{6}$$

where F_C, F_D and F_M are the total, DME and methanol carbon molar flow rates, respectively.

At this point it is important to clarify that conversion of oxygenates (DME and methanol) was defined as the scope conversion, for olefins are produced from both. In other words, it is of no interest the amount of DME that converts to methanol but the conversion that yields olefins or its subsequent secondary products.

Yield of lump i: It was defined as the ratio of moles of lump i formed (expressed in carbon moles) to moles of carbon fed.

$$Y_i = \frac{F_i}{F_C} \tag{7}$$

Selectivity of lump i: It was defined as the molar carbon rate formed of such lump per mole of carbon reacted:

$$S_i = \frac{F_i}{F_C - F_D - F_M} = \frac{Y_i}{X} \tag{8}$$

3.5. METHODOLOGY

3.5.1. Data analysis

A widely proven procedure for kinetic modelling by Toch et al. (2015) was followed. It entails three main stages (Data analysis and model construction, regression and physical assessment) yet a fourth stage concerning model discrimination was also covered.

Data analysis and model construction is the primal stage, prior to establishing a kinetic model. Toch and co-workers (2015) highlight the importance of analysing experimental results so as to being truly aware of the information they represent by, for example, plotting dependant variables (most distinctive ones are conversion, yield and selectivity) as function of independent variables (such as temperature or space time). From the knowledge acquired, complemented with literature research, reaction steps and reaction rates can be defined. At this point, employment of pseudo-components or reaction families -lumps- as a form of reducing reaction rates and parameters involved in the network is suggested.

The second stage encompasses the regression of model derived results with respect to experimental ones. Kinetic models are usually non-linear, and consequently, as a rule of thumb, accurate initial guesses are recommended. Otherwise, there are high chances of the objective function optimisation routine ending at local maxima/minima. The objective function should be carefully defined in accordance with the problem formulation and may require the introduction of weights.

Then, parameter evaluation is done. Evaluating the parameters means ensuring they have a proper physical meaning, which can be done, for instance, by checking that deactivation order is within reasonable values according to literature.

The last step of the methodology followed includes statistical analyses of the models used and model discrimination. By studying the statistical significance of each model, the best model available can be determined.

3.5.2. Modelling procedure

Kinetic modelling primarily consisted of solving the conservation equation for all of the lumps involved in the reaction system and matching results with experimental data using an in-house MATLAB code. Such endeavour involved integrating the conservation equation by means of a finite approach 4th order Runge-Kutta method, a multivariable non-linear regression with the Levenberg-Marquardt algorithm and Fisher test and variance analyses for model significance and discrimination.

<u>Conservation equation</u>

The core of the model is the conservation equation which was formulated for each of the lumps present in the reaction medium. Due to the remarkable deactivation of the catalyst that takes place during the reaction for certain operating conditions, the conservation equation must be conceived as a function of time.

On the other hand, since the observed head loss is negligible, it was considered reasonable to assume a constant pressure. Radial concentration and temperature gradients were also considered to be negligible, the latter being contrasted with the data provided by the thermocouples present in the bed. With these conditions, the conservation equation for a dl infinitesimal reactor length:

$$\varepsilon_b P \frac{\partial y_i}{\partial t} = -vP \frac{\partial y_i}{\partial l} + D_e \frac{\partial^2 y_i}{\partial l^2} + \rho_b r_i RT \tag{9}$$

where ε_b is the effective bed-particle porosity, P is the total pressure, y_i is the molar fraction (expressed in carbon units) of a lump i, t is the time, l is the bed length, v is the bulk velocity, De is the effective dispersion coefficient, ρ_b is the bed density, r_i is the formation rate of the lump i, R is the universal gas constant and T is the reactor temperature.

Time dependant term corresponds to accumulation, whereas right-hand side terms in equation (9) represent, from left to right, mass transport due to convection, dispersion and reaction, respectively. The diffusional effect was deemed significantly smaller with respect to the rest, due to the high Peclet number obtained (for mass transfer, Peclet is defined as the product of Reynolds number by Schmidt number, representing the ratio of convective to molecular transport) (Seader et al., 2011). Thus, it was neglected. So, and as ideal gas law applied:

$$\frac{P}{RT}\varepsilon_b \frac{\partial y_i}{\partial t} = -\frac{F_T}{S}\frac{\partial y_i}{\partial l} + \rho_b r_i \tag{10}$$

where S is the reactor section and F_T is the total molar flow rate. Shall the ratio of carbon molar flow rate to total molar flow rate be defined:

$$N_C = \frac{F_C}{F_T} \tag{11}$$

Whence:

$$\frac{P}{RT}\varepsilon_b N_C \frac{\partial y_i}{\partial t} = -\frac{F_C}{S}\frac{\partial y_i}{\partial l} + \rho_b r_i \tag{12}$$

Besides, r_i was defined as:

$$r_i = \frac{dy_i}{d\left(\dfrac{W}{F_C}\right)} = \frac{dy_i}{d(\tau)} \tag{13}$$

where W is catalyst mass and τ is space time.

Since several reactions are involved in the process, reaction rates involved for a step j in the reaction scheme (r_j) had to be defined. As a matter of fact, r_j is the product of the multiplication between $r_{j,0}$ and the activity of the catalyst (a). Indeed, $r_{j,0}$ is the reaction rate at time 0 (without deactivation) of the step j and was determined by law of mass action (concentration of each compound in terms of partial pressure) together with a θ factor, as shown in the following equation:

$$r_j = r_{j,0}a = k_j P_R^{n_R}\theta a \tag{14}$$

where R represents reacting lumps in the step j, n_R is the reaction order of R, k_j is the kinetic constant of the step j and θ is the factor representing reaction attenuation by water and methanol adsorption in catalyst acidic sites.

Equation (14) complies to scenarios where only one activity exists (non-selective deactivation), in which all reaction steps are affected by the same activity a., like the ones contemplated in the paper. However, models with more activities do also exist (selective deactivation).

Regarding θ, despite a handful of papers (Gayubo et al., 2003; Ying et al., 2015) suggest that only water attenuates reaction progress, Pérez-Uriarte and co-workers (2017) state that methanol plays a role too in DTO runs and so was considered for the model:

$$\theta = \frac{1}{1 + K_a\left(P_M + P_W\right)} \tag{15}$$

where K_a is a parameter that quantifies the adsorption of both methanol and water (hence their partial pressures involved) and follows the next equation:

$$K_a = K_a^* \exp\left[-\frac{\Delta H_a}{R}\left(\frac{1}{T} - \frac{1}{T^*}\right)\right]$$ (16)

where K_a^* is the value of K_a at the T^* reference temperature (350 °C) and ΔH_a is the apparent adsorption heat of methanol and water.

Besides, r_i and r_j were related as follows:

$$r_i = \sum_j (v_i)_j \, r_j$$ (17)

where $(v_i)_j$ is the carbon balance coefficient of the lump i in the reaction step j of the kinetic scheme, and r_j is the reaction rate of the reaction step j.

Simultaneously, r_d was defined as the deactivation rate of each of the catalyst activities present in the model. For non-selective deactivation equations, r_d is just a function of the only existing activity. Deactivation rates were defined with a particular expression as a function of the reaction temperature and the concentration (partial pressure) of the coke precursors, P_{cp}, as shown in the next equation:

$$r_d = -\frac{da}{dt} = k_d \sum_{cp} P_{cp} \, \theta_d a^d$$ (18)

where k_d represents deactivation kinetic constant present in the deactivation equation, d is the order of the deactivation equation and θ_d is a term that quantifies the attenuation of the deactivation by the adsorption of water (Gayubo et al., 2003; Pérez-Uriarte et al., 2017; Ying et al., 2015). The latter follows:

$$\theta_d = \frac{1}{1 + K_{W,d} P_W}$$ (19)

where $K_{W,d}$ is a parameter that quantifies the adsorption of water (hence its partial pressure involved) and follows the next equation:

$$K_{W,d} = K_{W,d}^* \exp\left[-\frac{\Delta H_{W,d}}{R}\left(\frac{1}{T} - \frac{1}{T^*}\right)\right]$$ (20)

where $K_{W,d}^*$ is the value of $K_{W,d}$ at the T^* reference temperature (350 °C) and $\Delta H_{W,d}$ is the apparent adsorption heat of water.

In the reaction rates (Eq. (14)) and deactivation rates (Eq. (18)) explained kinetic parameters (k_j and k_d) were noticeable partaking variables. At this point is worth explaining that a reparametrised Arrhenius describes them:

$$k = k^* \exp\left[-\frac{E}{R}\left(\frac{1}{T} - \frac{1}{T^*} \right) \right] \qquad (21)$$

where k is the kinetic constant term covering k_j and k_d, k^* is the kinetic constant term (comprising k_j^* and k_d^*) at the reference temperature T^* (350 °C) and E is the activation energy term that includes activation energies for each of the k_j (E_j) and k_d (E_d) present in the deactivation equation.

Integration and boundary conditions

The conservation equations for each lump can be classified as a system of parabolic partial differential equation, but it was transformed into a system of ordinary differential equations (ODEs) in order to simplify its solution. ODEs were integrated using an implicit Runge-Kutta method based on the numerical differentiation formulas of orders 1–5. Like with any ODE, integration required setting boundary conditions that enabled finding the characteristic solution. Such conditions are:

$$y_i(t = 0, l) = y_{i,0} \qquad (22)$$

$$a(t = 0, l) = 1 \qquad (23)$$

$$y_i(t, l = 0) = y_{i,in} \qquad (24)$$

where $y_{i,0}$ and $y_{i,in}$ are the molar fractions of the lump i at zero-time on stream and at the inlet of the reactor, respectively, expressed in carbon units. Therefore, Equations (22) and (23) refer to a system with a non-deactivated catalyst (t=0). That is, they are related in that as a consequence of the activity being 1 at t=0, the fractions of the lumps are those that correspond to a catalyst without deactivation. The third condition, on the other hand, reflects that the composition of the feed during the whole experiment is constant, as it was done in the laboratory.

Algorithm

Kinetic parameters were calculated by means of the Levenberg-Marquardt algorithm. This algorithm is the result of the combination of the Gradient decent and Gauss-Newton methods for searching function extrema, frequently used for solving problems of nonlinear least square minimisation (Marquardt, 1963). Gradient descent algorithm is founded on finding maxima/minima of functions from a starting point by following the path with biggest slope. The Gauss-Newton method, however, consists of minimising the sum of the squares of the residuals between data and nonlinear equations, expressing the original nonlinear equation in an approximate, Taylor series expansion linear form (Chapra and Canale, 2010).

The Gradient descent is known to increase the value of the objective function however far the initial guess might be, whereas the Gauss-Newton algorithm rapidly converges when near to the optimum point. So, Levenberg-Marquardt method offers the best of both by hessian evaluation and matrix inversion at each step. Indeed, it is reliable if poor initial starting values are provided and accelerates rapidly when it approaches the optimum (Chapra and Canale, 2010).

A modified version of the mentioned algorithm was used on account of being able to solve nonlinear differential equations and various objective functions at the same time (multiobjective algorithm). The latter is crucial, for the non-modified Levenberg-Marquardt algorithm faces problems where two objective functions are needed by solving them one after the other. In the problem studied, it would have minimised the first objective function to obtain the intrinsic kinetic parameters (without deactivation). With the intrinsic parameters, then, it would have solved the second objective function to calculate the deactivation parameters. Therefore, the error associated to the intrinsic parameters would have been propagated to the calculation of the second ones (Cordero-Lanzac et al., 2018); such thing does not occur when working with multiobjective algorithms like the modified Levenberg-Marquardt, for it was able to solve two objective functions in parallel. The parallel objective functions written to be minimised are as follows, which were grouped within a target objective function:

$$OF = \begin{bmatrix} \sum_{i=1}^{n_l} \sum_{n=1}^{n_{e,0}} \frac{R_n}{n_{e,0}} \left(y_{i,n}^{0*} - y_{i,n}^{0} \right) \\ \sum_{i=1}^{n_l} \sum_{n=1}^{n_{e,d}} \frac{R_n}{n_{e,d}} \left(y_{i,n}^{t*} - y_{i,n}^{t} \right) \end{bmatrix} \tag{25}$$

where: n_l is the number of lumps, R_n is the number of runs repeated at the same conditions and $n_{e,0}$ and $n_{e,d}$ are the total number of experimental data used for the calculation of the first and second term of the OF, respectively.

$y_{i,n}^{0*}$ and $y_{i,n}^{t*}$ are the experimental molar fractions of the lump i corresponding to zero time on stream and at t time on stream and $y_{i,n}^{0}$ and $y_{i,n}^{t}$ are molar fractions of the lump i obtained by kinetic model integration. Thereby, it remains clear that the first function of the OF belongs to non-deactivation kinetic parameters (intrinsic), whereas the second enables deactivation kinetic parameter calculations.

Significance and discrimination

The more complex models tend to yield better results, but many times, the improvement is not worth the added complexity it entails. When that happens, the improvement is deemed insignificant. Therefore, determining the significance of the improvements made by different models for choosing the most appropriate model is fundamental. That was done by significance tests and model discrimination. To ease such analyses, the sum of square errors was defined which is the sum of the square difference between experimental and model based lump molar fractions at zero time and TOS:

$$SSE = \sum_{i=1}^{n_l} \left[\sum_{n=1}^{n_{e,0}} \left(y_{i,n}^{0*} - y_{i,n}^{0} \right)^2 + \sum_{n=1}^{n_{e,d}} \left(y_{i,n}^{t*} - y_{i,n}^{t} \right)^2 \right] \tag{26}$$

If two models (A and B) with the same number of degrees of freedom ($\nu_A = \nu_B$) were to be compared, the model discrimination was done by evaluating the ratio of the variances of both models. Variances of A and B (s_A^2 and s_B^2) were calculated as the ratio of the corresponding values of the sum of square errors (SSE_A and SSE_B, respectively) and degrees of freedom. So, given $s_A^2 > s_B^2$, it can be said that model B brought significant improvements with respect to A if the following inequality was met (Mier et al., 2010; Pérez-Uriarte et al., 2017):

$$F_{A-B} = \frac{\dfrac{SSE_A}{\upsilon_A}}{\dfrac{SSE_B}{\upsilon_B}} = \frac{s_A^2}{s_B^2} > F_{1-\alpha}\left(\upsilon_A, \upsilon_B\right) \tag{27}$$

where $F_{1-\alpha}$ is the critical value of the Fisher distribution function calculated, in this case, using the MATLAB *finv* function. The critical value of the Fischer distribution function is a function of the degrees of freedom for the variances compared (A, B) and of the percentage of confidence sought for the comparison, 100 (1-α).

On the other hand, if models being compared (A and B) had different degrees of freedom, in the case that $\upsilon_A > \upsilon_B$ and consequently $SSE_A > SSE_B$ (otherwise no further discussion proceeded), model B represented only a significant improvement if:

$$F_{A-B} = \frac{\dfrac{SSE_A - SSE_B}{SSE_B}}{\dfrac{\upsilon_A - \upsilon_B}{\upsilon_B}} > F_{1-\alpha}\left(\upsilon_A - \upsilon_B, \upsilon_B\right) \tag{28}$$

4. RESULTS AND DISCUSSION

4.1. EFFECT OF REACTION CONDITIONS

4.1.1. Conversion

Figure 8a depicts the effect space time has on the conversion as a function of temperature for a pure DME feed (solid lines) and zero time. As expected, a significant improvement in conversion of oxygenates is observed when increasing both temperature and space time. Indeed, for a space time of 0.5 g_{cat} h mol_C^{-1}, a 50 ºC difference in temperature (from 325 ºC to 375 ºC) raises conversion from an almost neglectable 6% to 48%. At the same time, for a given temperature when pure DME was fed, it is observed that a nearly linear trend (not applicable when complete conversions are approached) exists between conversion and space time. In fact, the slope of that virtual linearity is quite prominent, as conversion shifts from 23% to 50% when space time is doubled (from 1 g_{cat} h mol_C^{-1} to 2 g_{cat} h mol_C^{-1}) at 350 ºC, a 113% rise.
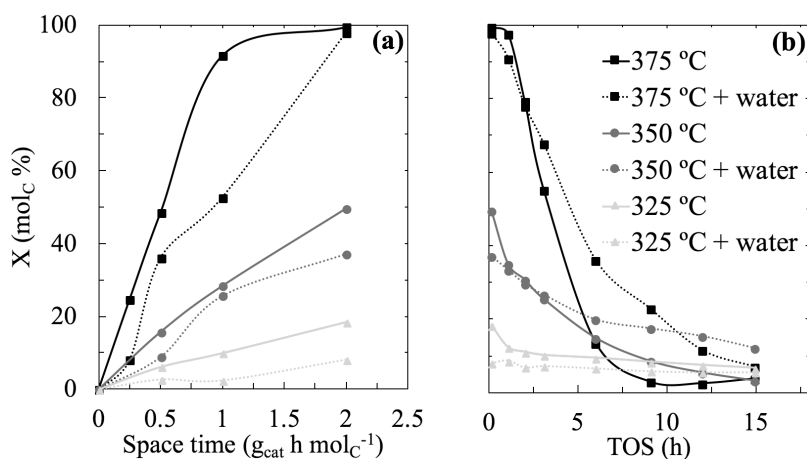

Figure 8. Effect of temperature and co-feeding water on the evolution of the conversion with (a) space time (at TOS = 0) and (b) time on stream (at 2 g_{cat} h mol_C^{-1})

The time-dependent deactivation of the HZSM-5 catalyst in the fixed reactor at 2 g_{cat} h mol_C^{-1} is shown in Figure 8b. Different temperature results in different deactivation tendencies for a pure DME feed (solid lines). For temperatures evolution of conversion with TOS shows a completely decreasing exponential behaviour. However, as temperature values increase, the decreasing exponential feature is delayed. In fact, for 375 ºC and a pure feed, a maximum conversion is detected preceding an inflexion point that leads to an abrupt exponential decrease, as a consequence of the great amount of catalyst (hence no deactivation) in the reactor. It is also noteworthy that conversions at all temperatures asymptotically approach the same value at high TOS (>10 h), thus implying that at greater space times deactivation rate is higher, given at zero-time conversions at bigger space times are way bigger (more prominent decreasing slope).

In both Figures 8a and 8b solid lines and dashed lines represent pure DME feed and DME + water mixture feed (ratio of 1mole H_2O fed per C mole fed) respectively. By examining Figure 8a, it remains crystal clear that co-feeding water attenuates progress of reactions, given that for all conditions depicted in such figure, conversions when co-feeding are always below those belonging to a pure feed. On the other hand, from Figure 8b a major conclusion can be drawn if both feeds are compared: water hinders deactivation as conversions (of the feed containing water) are higher for most of the TOS (at any space time). Nonetheless, at lowest TOS values

(<2 h), greater conversions are observed for the pure feed, which means at that TOS, the effect of water for attenuating progress of reactions is bigger than its effect of hindering deactivation. Thus, it could be stated that the effect of water in reaction mitigation is comparable to the drop of activity associated to the very early stages of deactivation when feeding pure DME.

4.1.2. Yield

Figure 9a portrays how space time affects product distribution expressed as yield, for a pure DME feed at 375 °C and zero time. Every lump -with the exception of olefins- shows an ascendant trend with space time. The olefin yield goes through a maximum located at a space time of 1 g_{cat} h mol_C^{-1}, which can be understood as if olefins were intermediates (in secondary reactions) in the kinetic scheme. It should be noted that under the conditions displayed, the concentrations of methane and CO_x and CH_4 are very small.
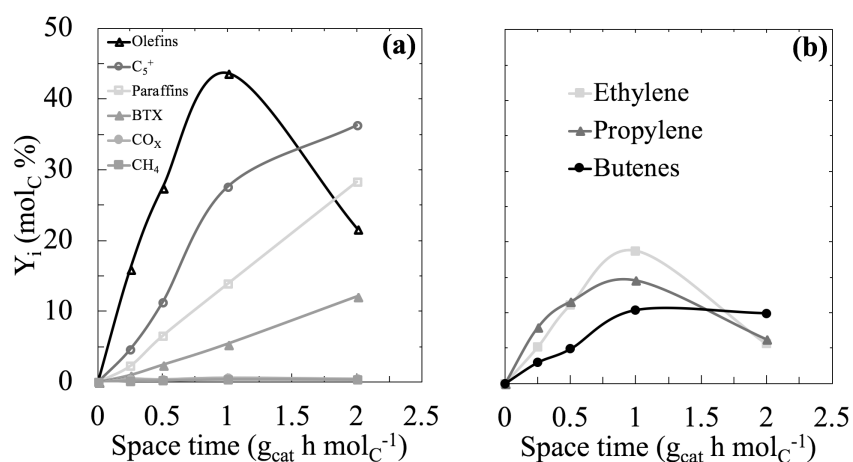

Figure 9. Evolution with the space time of the yield for a pure DME feed (a) of product and by-product lumps and (b) of components of the olefin lump (375 °C, TOS = 0).

Figure 9b displays the evolution of the yield of the components of the olefin lump (ethylene, propylene and butenes) for the conditions explained for Figure 9a. The most remarkable feature of Figure 9b is that ethylene and propylene are the compounds responsible for the trend of the olefin lump with space time explained before. They both undergo a maximum that is then reflected on the lump maximum. Same does not apply to the butenes, whose yield remains constant when ethylene and propylene start to decay. As a whole, by examining yields at a given temperature, it can be concluded that an optimal space time exists for maximising target olefins.

4.1.3. Selectivity

Figure 10a displays how co-feeding water affects both conversion and selectivity of the products. As it can be seen, for same conditions of temperature and space time, water in with DME attenuates oxygenates conversion and at the same time enhances desired light olefin selectivity. Actually, light olefin selectivity rises while a decrease in the content of secondary products, especially of paraffins and aliphatics is observed, just as Gayubo et al. (2004) reported.
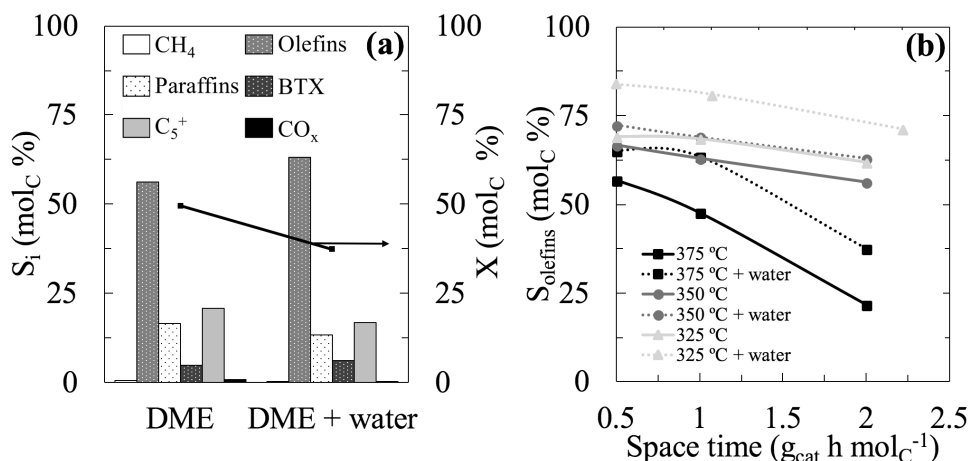
Figure 10. Effect of water with DME (a) on selectivity of products and conversion (T=350 ºC, space time=2 g_{cat} h mol_C^{-1} and TOS=0 h) and (b) on the evolution of selectivity of olefins at zero time.

Besides, Figure 10b presents, at zero time, how olefin selectivity changes with both space time and temperature. It remains clear that olefin selectivity falls as both variables are augmented. Actually, it has been observed that such decrease in selectivity implies an opposite trend for paraffins, aliphatics and other by-products, suggesting that when increasing space time and/or temperature, secondary reactions (like hydrogen transfer or oligomerisation) are boosted. In addition, conclusions from Figure 10a are confirmed, for dashed lines representing water co-feeding in Figure 10b result in higher light olefin selectivity than solid lines representing a pure feed.

4.2. PROPOSED MODELS

4.2.1. Intrinsic reaction scheme

Synthesis of desired olefins from DME is explained by DME hydrolysis and double cycle mechanism, as it has previously been explained. Six major steps take part in that mechanism: olefin methylation, higher olefin cracking, hydrogen transfer and cyclisation (these conforming the olefin cycle) and aromatic methylation and dealkylation (these correspond to the arene cycle).

DME hydrolysis reaction and double cycle mechanism are therefore to be represented in the reaction scheme used for zero time, which is assumed to encompass 10 steps. These are written in Figure 11 and graphically shown in Figure 12. Despite that, other factors were also considered when stating the model, like physical sense (e.g. matching products observed experimentally to those predicted by the model) and simplicity were also key when stating the scheme. In other words, the reaction scheme is a hybrid of both.
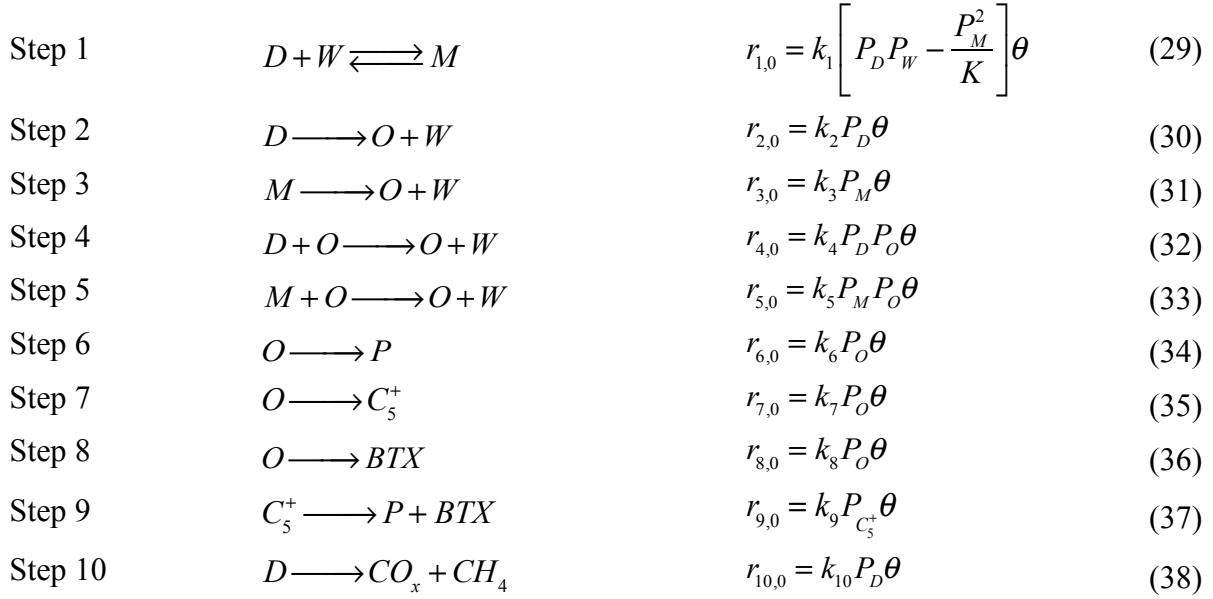
Step 1	$D + W \rightleftarrows M$	$r_{1,0} = k_1 \left[P_D P_W - \dfrac{P_M^2}{K} \right] \theta$	(29)
Step 2	$D \longrightarrow O + W$	$r_{2,0} = k_2 P_D \theta$	(30)
Step 3	$M \longrightarrow O + W$	$r_{3,0} = k_3 P_M \theta$	(31)
Step 4	$D + O \longrightarrow O + W$	$r_{4,0} = k_4 P_D P_O \theta$	(32)
Step 5	$M + O \longrightarrow O + W$	$r_{5,0} = k_5 P_M P_O \theta$	(33)
Step 6	$O \longrightarrow P$	$r_{6,0} = k_6 P_O \theta$	(34)
Step 7	$O \longrightarrow C_5^+$	$r_{7,0} = k_7 P_O \theta$	(35)
Step 8	$O \longrightarrow BTX$	$r_{8,0} = k_8 P_O \theta$	(36)
Step 9	$C_5^+ \longrightarrow P + BTX$	$r_{9,0} = k_9 P_{C_5^+} \theta$	(37)
Step 10	$D \longrightarrow CO_x + CH_4$	$r_{10,0} = k_{10} P_D \theta$	(38)

Figure 11. Steps of the proposed reaction scheme and their reaction rates equations.

where D, W, M, O, P, C_5^+, BTX, CO_x and CH_4 correspond to the DME, water, methanol, olefins, paraffins, C_5^+ aliphatics, aromatics, $CO + CO_2$ and methane lumps, respectively.
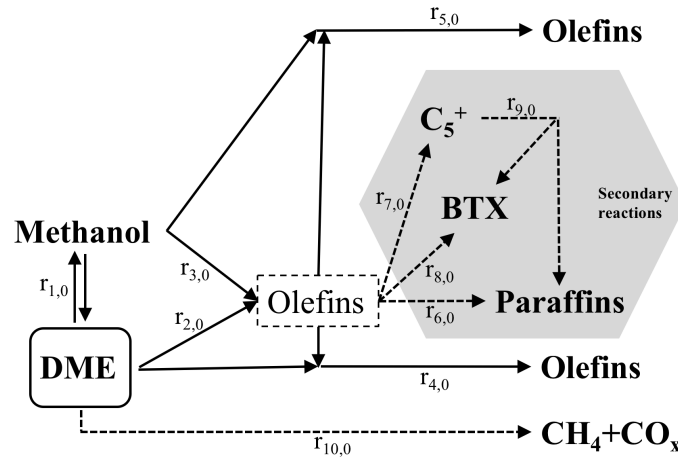

Figure 12. Graphical summary of the 10 reaction steps forming the intrinsic reaction scheme.

All of the 10 steps conforming the reaction scheme at zero time were assumed to be elementary, hence their order of reaction was calculated straightforward. Partial pressures, to the power of the elementary reaction order, act as concentration quantifiers. At this point, it is worth clarifying that steps in Figure 11 are written in carbon units; therefore, in the case of step 4 for instance, it implies that one mole of carbon from DME and another from the existing olefins yield two olefin carbon moles and water. Furthermore, the carbon balance coefficients mentioned in Eq. (17) for that step would be: DME (-1), olefins (1) and water (1). In the case of water, a coefficient based on the moles of water formed per mole of carbon reacted is defined.

Step 1 (Eq. (29)) represents DME hydrolysis reaction, in which the DME, water and methanol equilibrium mixture is formed. It is essentially the methanol dehydration reaction. Indeed, concerning DME formation in methanol dehydration, different mechanisms have been proposed as Jiang et al. (2004) mention. One suggests that reaction of methanol occurs at the

Brønsted acidic and its adjacent Lewis basic sites by the formation of the two partaking surface species $[CH_3 \cdot OH_2]^+$ and $[CH_3O]^-$ which through condensation result in DME and water.

It is worth mentioning that step 1 has the same term as any other step in Figure 11 for indicating the hindering effect water and methanol have on the progress of the reaction (θ). θ implies a 1st order hyperbolic effect of water and methanol attenuation for the DME hydrolysis reaction, despite what Sierra et al. (2013) observed. After comparing various models (exponentials and hyperbolics) with different partaking species, they stated that the exponential attenuation of DME, methanol and water fitted better. Anyhow, with the purpose of not adding even more complexity to the model, a single θ expression for all steps comprising the model was used, represented in Equation (15).

DME-methanol equilibrium is known to be the quickest of all 10 steps involved, and its equilibrium has been widely studied because it plays a key role in DME synthesis from syngas. Aguayo and co-workers (2007) provided an exponential equation for the equilibrium constant, which is only temperature dependant (pressure has no effect on it whatsoever owing to the null variation of moles in the reaction). As they elucidated, its coefficients were calculated from the standard values of formation enthalpies and entropies of the components participating in the hydration reaction. The equation for the equilibrium constant is the following:

$$K = \frac{k_1}{k_{-1}} = \exp\left[-9.76 + \frac{3200}{T} + 1.07\log T + 6.6\ 10^{-4}T + 4.9\ 10^{-8}T^2 + \frac{6500}{T^2}\right] \tag{39}$$

Steps 2 and 3 (Eqs. (30-31)) depict how the feed, in its original DME form or in its hydrolysed methanol form, is converted to olefins. It a way of expressing that the feed (by addition of methyl groups) forms olefins. In such methylation process, reactants go through aromatic intermediate species which were of no interest when modelling kinetics. Indeed, for steps 2-9 (Eqs. (30-37)), it is fundamental to mention that they only take into account the overall initial and final species taking part in each of the steps, ignoring the intermediates that might be formed within the process.

Steps 4 and 5 (Eqs. (32-33)), on the other hand, represent the autocatalytic nature of the double cycle mechanism. These are autocatalytic reactions where olefins react with the methyl groups provided by the feed (in step 4 coming from DME and in step 5 coming from methanol) to yield more olefins and water. In a certain way, steps 2-5 comprise the complete double cycle mechanism to form olefins with its 6 steps contained within these steps, many of which only involve intermediate species (and therefore not shown).

Steps 6-9 (Eqs. (34-37)) explain how by-products are formed through secondary reactions. Some by-products are foreseen by the double cycle mechanism, such as the C_5^+ aliphatics in the form of paraffins. Some others (BTX or lower paraffins), however, are not, but the scheme needs to predict them so that it can result in a proper data fitting.

Steps 6-8 imply that olefins can eventually yield C_2-C_4 ranged paraffins, aromatics and C_5^+ aliphatics. Paraffins and aromatics are formed by means of hydrogen transfer and condensation reactions, whereas olefins undergo oligomerisation reactions to form aliphatics. In this case as well, little attention was paid to the pathway by which the mentioned by-products are formed; anyhow, it is known that in the case of aliphatics formation, olefins form intermediate polyalkylbenzenes, which subsequently methylate to later crack into a C_5^+ aliphatic species.

Step 9, besides, explains C_5^+ aliphatic cracking and aromatisation, with the formation of C_2–C_4 paraffins and aromatics.

Lastly, step 10 (Eq. (38)) shows the DME thermal decomposition reaction where CH_4 and CO_x are formed, as a way of justifying the presence of methane and CO_x species in the reaction medium. This reaction is, kinetically speaking, the most unimportant reaction of all, for methane and CO_x yields are the lowest, at tested temperatures. Nevertheless, it ought not to be underrated, because it is a reaction in which part of the feed is wasted.

In accordance with the literature searched, two main features are to be highlighted. On the one hand, Gayubo et al. (2004) reported that DME and methanol have dissimilar reactivities, suggesting that they should be separately treated; their lumping was done accordingly. On the other hand, Pérez-Uriarte and co-workers (2017) stated that if C_2-C_4 olefins are treated on their own, better model fitting results. In spite of it, a simpler strategy was adopted for physical meaning and ease of calculations. Thereby, in the work, an olefin lump encircling all C_2-C_4 olefins was defined.

4.2.2. Deactivation equations

The deactivation equations tested in the work (for the reaction scheme already proposed) are quasi non-selective equations, where a single activity was employed. The group of quasi non-selective deactivation equations embodies those accounting for a single activity, yet they were considered quasi non-selective (instead of non-selective as stated before) because the activity term did not apply to the thermal decomposition of the DME (step 10 in Figure 11).

There are many examples in literature in which small paraffins (mostly CH_4), CO and CO_2 appear in the product spectrum without being species involved in the main reactions. Depending on the case, it can be mechanistically explained (Cordero-Lanzac et al., 2018), but some other times, cracking due to temperature of the hydrocarbon feed has to be considered (Aguayo et al., 2010; Pérez-Uriarte et al., 2017). Even when it is mechanistically explained, little yields lead to think of the thermal cracking theory. Anyway, as the decomposition occurs because of the physical nature (and not catalytic) of the reaction, it is recurrent to avoid using the activity term in its reaction rate expression. That is why quasi non-selective deactivation equations are broadly used in the literature (Cordero-lanzac et al., 2018; Pérez-Uriarte et al., 2017).

So, when quasi non-selective deactivation equations are used, reaction rates for all the steps -except for the thermal decomposition (step 10 in Figure 11) which has no activity term- are calculated from the multiplication of reaction rates of each step at zero time and the activity, as explained in Equation (14). For what has just been stated, neither CO_x nor CH_4 could be considered as coke precursors. Under that premise, 8 deactivation equations were proposed for the reaction scheme in Figure 11. The deactivation equations are shown in Table 3.

Table 3. Proposed kinetic equations for a quasi non-selective catalyst deactivation.

Equation	Coke precursor	Deactivation equation	
A	All species	$$-\frac{da}{dt} = k_d\left(P_D + P_O + P_P + P_{BTX} + P_{C_5^+} + P_M\right)\theta_d a^d$$	(40)
B	DME & Hydrocarbons	$$-\frac{da}{dt} = k_d\left(P_D + P_O + P_P + P_{BTX} + P_{C_5^+}\right)\theta_d a^d$$	(41)
C	Oxygenates	$$-\frac{da}{dt} = k_d\left(P_D + P_M\right)\theta_d a^d$$	(42)
D	DME	$$-\frac{da}{dt} = k_d P_D \theta_d a^d$$	(43)
E	Hydrocarbons	$$-\frac{da}{dt} = k_d\left(P_O + P_P + P_{BTX} + P_{C_5^+}\right)\theta_d a^d$$	(44)
F	All species	$$-\frac{da}{dt} = \left[k_{d1}P_D + k_{d2}\left(P_O + P_P + P_{BTX} + P_{C_5^+} + P_M\right)\right]\theta_d a^d$$	(45)
G	All species	$$-\frac{da}{dt} = \left[k_{d1}\left(P_D + P_M\right) + k_{d2}\left(P_O + P_P + P_{BTX} + P_{C_5^+}\right)\right]\theta_d a^d$$	(46)
H	DME & Hydrocarbons	$$-\frac{da}{dt} = \left[k_{d1}P_D + k_{d2}\left(P_O + P_P + P_{BTX} + P_{C_5^+}\right)\right]\theta_d a^d$$	(47)

In equation A (Eq. (40)), deactivation is considered to be independent of the progress of the reaction, since it considers that coke is formed at any time by any species present in the reaction medium. Deactivation equation B (Eq. (41)), however, albeit being similar to equation A, differs from it in that methanol is not considered to be a coke precursor. Thereby, according to equation B, the more DME is hydrolysed to methanol (for the same hydrocarbon yield attained in equation A), the milder the deactivation is. Somehow, it can be stated that equation B considers an in-series/in-parallel deactivation.

Looking at equation C (Eq. (42)), catalyst deactivation increases upon increasing oxygenates concentration and therefore, oxygenates are considered to be the unique coke precursors. So, it can be understood as if coke formation occurs strictly in parallel with the formation of the hydrocarbon species from oxygenates. Besides, the only variation observed from equation C to equation D (Eq. (43)) is that the latter does not consider both oxygenates to be coke precursors but just DME. Then, equation D encircles an in-parallel based deactivation equation which neglects the role methanol plays in forming coke.

Equation E (Eq. (44)) predicts that coke can only start to appear after oxygenates have been converted to hydrocarbons, thus coke formation taking place in series with oxygenates conversion. Consequently, according to this, the hydrocarbon species formed -olefins, paraffins, aromatics and aliphatics- are the only precursors.

Equations A-E in Table 3 have only one deactivation constant. Therefore, in equations with more than one coke preceding species, all the carbonaceous components have the same capacity for coke formation, depending only on concentration in the reaction medium. That does not apply to equations F-H (Eqs. (45-47)), because by having two kinetic constants each, they are

capable of establishing two different contributions according to the role each lump plays (or pathway it follows) in the deactivation process.

Indeed, equation F has same coking species involved as equation A, but the importance of the role of DME is set to be different from the rest. Similarly, equation G not only does recognise DME as a species of different role than the rest, but also extends that to methanol by grouping them together under k_{d1}. In other words, it considers that the in-parallel coke formation configuration undergoes a different pathway compared to the rest of the hydrocarbon products (the in-series coke formation). Equations B and H are related in the exact way that equations A and F are.

4.2.3. Kinetic model definition

From the combination of the reaction scheme with each of the deactivation equations presented in Table 3, kinetic models were formed. Nomenclature used for deactivation equations propounded (A-H) were maintained (so, models were named A-H as well). As an example, by the combination of the reaction scheme with deactivation equation A, kinetic model A resulted, and so on. It is to be highlighted that some of the parameters involved in the models corresponded to the reaction scheme (k_j^*, E_j, K_a^*, ΔH_a), whereas others came from the deactivation equations (k_d^*, E_d, d, $K_{W,d}^*$, $\Delta H_{W,d}$). Actually, the total number of parameters in a model is essentially the sum those coming from the reaction scheme and deactivation equation.

4.3. KINETIC MODEL DISCRIMINATION

Discrimination of deactivation equations was performed swapping its order with the physical meaning evaluation according to what explained in the general methodology, so that focus was set on the best models. Discrimination among the proposed models was done only for a pure DME feed.

4.3.1. Discrimination of models with one deactivation kinetic constant

Firstly, models with 783 degrees of freedom were studied. The number of degrees of freedom was calculated following the next equation:

$$\upsilon = \left(n_{e,0} + n_{e,d} \right) n_l - n_p \tag{48}$$

where n_p denotes the number of parameters present in the model.

All models presented coming from deactivation equations presented in Table 3 involve the same amount of total experiments ($n_{e,0}+n_{ed}=90$) and number of lumps ($n_l=9$). Then, models studied having the same number of degrees of freedom implies that they do also encircle the same number of parameters and hence, the same number of deactivation kinetic constants. To be more precise, all models of a single deactivation kinetic constant ($\upsilon=783$, $n_p=27$) were compared, as shown in Table 4. When only models with same number of degrees were involved, the statistic study of the significance of the improvement with the different models was evaluated by means of variance ratio analysis, as explained in Eq. (27). A confidence interval of 95% was established for every model. Model A, representing that all of the species in the reaction medium are coke precursors, was stated first. Models comprising all the species are usually defined first as an initial approach to the deactivation kinetics.

Table 4. Statistical comparison of models with a single deactivation kinetic constant (v=783).

Model	A	B	C	D	E
SSE	3.51 10^{-2}	3.21 10^{-2}	3.60 10^{-2}	3.70 10^{-2}	4.00 10^{-2}
s^2	2.68 10^{-3}	2.29 10^{-3}	2.92 10^{-3}	3.08 10^{-3}	2.22 10^{-3}
F	1.17 (F_{A-B})		1.05 (F_{D-C})	1.15 (F_{D-A})	1.03 (F_{B-E})
$F_{1-\alpha}$	1.12	1.12	1.12	1.12	1.12

Models A, C and D were studied firstly. Models C and D comprise the parallel deactivation configuration. So, by analysing the appropriateness of these, the importance of the in-parallel deactivation models could be determined. The remarkable significance of model A over D is supported by its corresponding Fisher test (1.15>1.12). Model C, on the other hand, shows unimportant improvement with respect to model D, according to statistics. In fact, although model C shows a lower SSE than model D, inequation from Eq. (27) not being met (due to a low variance ratio) favours model D over C (1.05<1.12). Straightforward, such comparison determines that A entails significant improvements with respect to model C as well. Thusly, in-parallel deactivation models were assumed not to be plausible, regardless of whether DME or both oxygenates are considered to be coke precursors.

Through comparison of models B and A, the importance of methanol as a coke precursor was judged since model B only differs from model A in that it does not conceive that methanol can directly influence catalyst deactivation. Model B is better at first glance, for it presents a flagrantly lower SSE than A. Such statement is confirmed when it is observed that the ratio of variances of models A and B is bigger than the critical value of the Fisher distribution (1.17>1.12). Thereby, the fact that methanol is not a source of coke was unconditionally assumed. Still, coke formation from methanol was expected to very limited on account of the small quantities of methanol detected in the reaction medium. In Figure 13 yields of methanol and other compounds are compared:
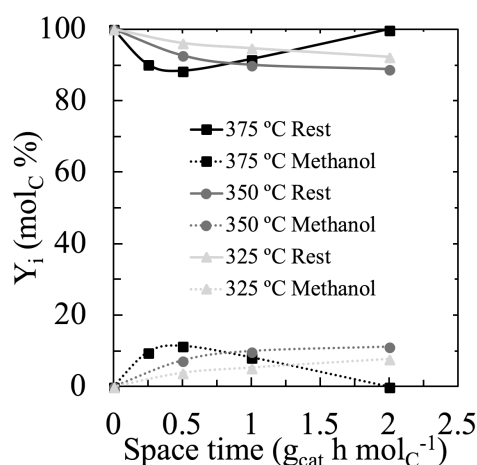
Figure 13. Effect of temperature on the evolution of the yield of methanol and the rest of compounds with the space time at TOS=0 h for a pure DME feed.

In Figure 13, zero time was represented because methanol yields decrease with TOS (since coke also hinders DME hydrolysis to methanol). For any other reaction condition represented, it can be observed how methanol yields are fairly low compared to the rest of the compounds. Note

that when both temperature and space time are high, the catalyst behaves so actively that a pseudo-state of fully conversion is attained, resulting in a nearly null methanol yield. When increasing either temperature or space time, in contrast, equilibrium towards methanol is favoured (for being an exothermic reaction) in the kinetic regime, wherein conversion is far from being complete, as shown in Figure 8a. Henceforth, the role of methanol in the deactivation was considered to be null.

Lastly, the effect of DME on the deactivation was studied. In order to do it, DME was removed as a coke preceding species from model B, resulting in model E in Table 3. Statistical analysis leaves no doubt about model E providing irrelevant improvement to the fitting, for the ratio of variances is lower than the critical value of the Fisher distribution (1.03<1.12). Furthermore, in model E SSE is significantly raised, showing the biggest SSE of all the models displayed in Table 4 (SSE_E=4.00 10^{-2}). As a result, a deactivation based on hydrocarbon products (in-series deactivation) was rejected as the definitive model for explaining catalyst deactivation.

To summarise, as it has been proven that deactivation models without methanol, in all cases, showed better quality of fitting than those contemplating it. Besides, purely in-parallel and purely in-series mechanisms for coke formation were determined to be inappropriate for describing deactivation. Such statement implies that models combining both sources of coke (from DME and products) display the deactivation phenomenon most accurately, which corresponds to model B from Table 4.

How model B fits under several different reaction conditions is shown by means of Figures 14 and 15. Note that the values of molar fractions of the products in this paper coincide with the yield of each product lumps. By observing them, it is perceived that model B provides a good overall quality of fitting, especially at zero time, yet that accuracy decreases at certain conditions of TOS such as high temperatures and low space times (Figure 15c). These conditions are often regarded as critical, as higher temperatures favour coke formation and its effect is magnified with lower catalyst mass (hence space time). In other words, coke easily blocks the pores of the HZSM-5, resulting in a very sensitive conversion over time. Thereby, improving the overall quality of the fitting model B provides (especially at the mentioned critical conditions) is the challenge faced.
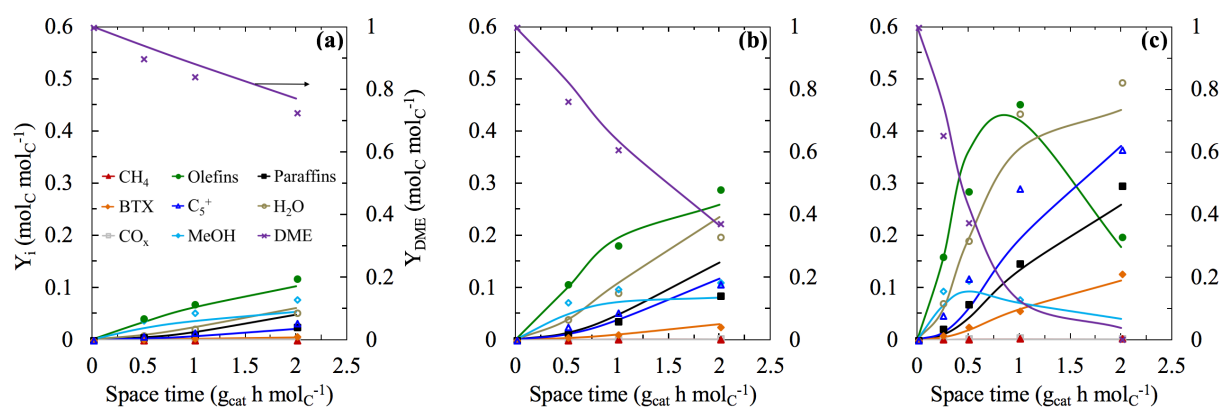

Figure 14. Comparison of the experimental data (dots) and those estimated with the kinetic model B (lines) for the evolution with space time of the product molar fractions for a pure DME feed at zero time on stream, at (a) 325 ºC, (b) 350 ºC and (c) 375 ºC.
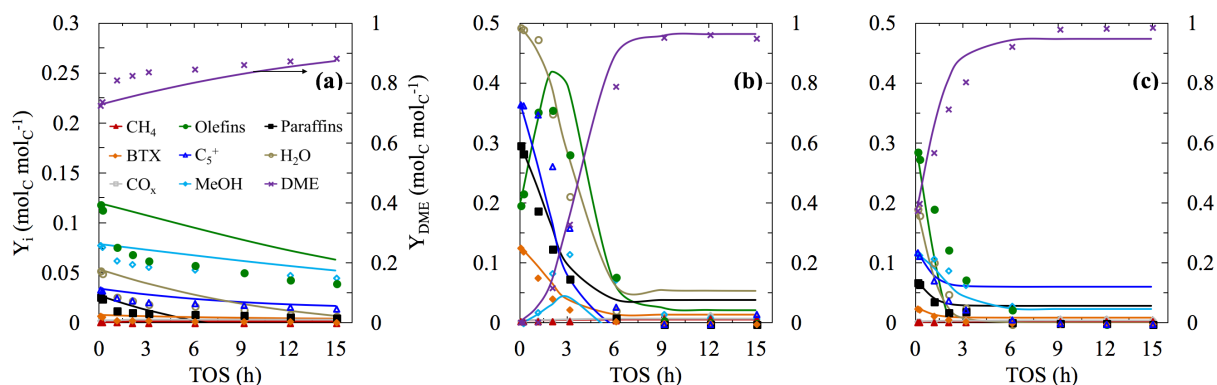
Figure 15. Comparison of the experimental data (dots) and those estimated with the kinetic model B (lines) for the evolution with time on stream of the product molar fractions for a pure DME feed at (a) 325 ºC and 2 g_{cat} h mol_C^{-1}, (b) 375 ºC and 2 g_{cat} h mol_C^{-1}, and (c) 375 ºC and 0.5 g_{cat} h mol_C^{-1}.

4.3.2. Discrimination of models with two deactivation kinetic constants

Afterwards, models with two deactivation kinetic constants were compared. These have 781 degrees of freedom, corresponding to the 29 parameters fixed by the addition of the second constant (Eq. (48)). It is to be noted that when stating these new models, no models C, D and E derived models were considered, for what they represent was previously proven to not be plausible. As done with models of a single deactivation kinetic constant, firstly, models involving all the species present in the reactor were taken into account. These are models F and G in Table 3.

Models F and G were rivalled (as depicted in Table 5) so as to determine whether a distinctive effect of DME over methanol exists. By variance ratio analysis (1.17>1.13 in Eq. (27)), model F is shown to fit to experimental data significantly better than model G, for a 95% confidence interval (besides having a lower SSE). Such outcomes proved that methanol was not to be coupled to DME as the latter follows a segregated pathway when forming coke.

Table 5. Statistical comparison of models with two deactivation kinetic constants (ν=781).

Model	F	G	H
SSE	3.35 10^{-2}	3.50 10^{-2}	3.08 10^{-2}
s^2	2.60 10^{-3}	3.05 10^{-3}	2.26 10^{-3}
F	1.15 (F_{F-H})	1.17 (F_{G-F})	
$F_{1-\alpha}$	1.13	1.13	

Before, removing methanol from the deactivation equation (from model A to B) resulted in a promising outcome. Accordingly, same was done with model F, from which model H derived. Both were compared, reaching a predictable conclusion. The statistic study of both models projects that model H brings a significantly better fitting to experimental data than model F (1.15>1.13). It is well known that in this case only variance ratio analysis applies, but model H showing a smaller SSE than any other model tested so far, is also a bright indicator about the significance of the improvement it entails. As a result, the irrelevance of the role methanol plays in deactivation remains was once more proved. A comparison between the experimental data

(dots) and the results predicted by model H (lines) of lump molar fractions in the outlet of the reactor at zero time on stream and TOS is displayed through Figures 16 and 17.
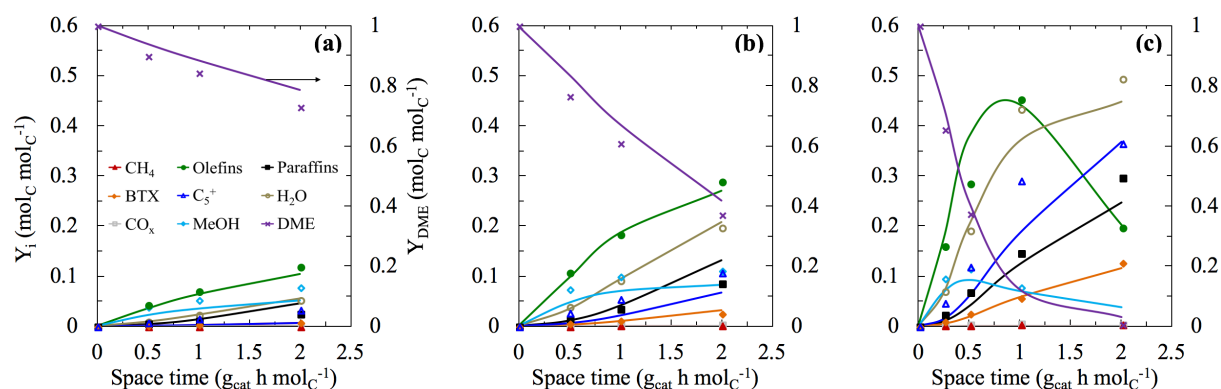

Figure 16. Comparison of the experimental data (dots) and those estimated with the kinetic model H (lines) for the evolution with space time of the product molar fractions for a pure DME feed at zero time on stream, at (a) 325 ºC, (b) 350 ºC and (c) 375 ºC.
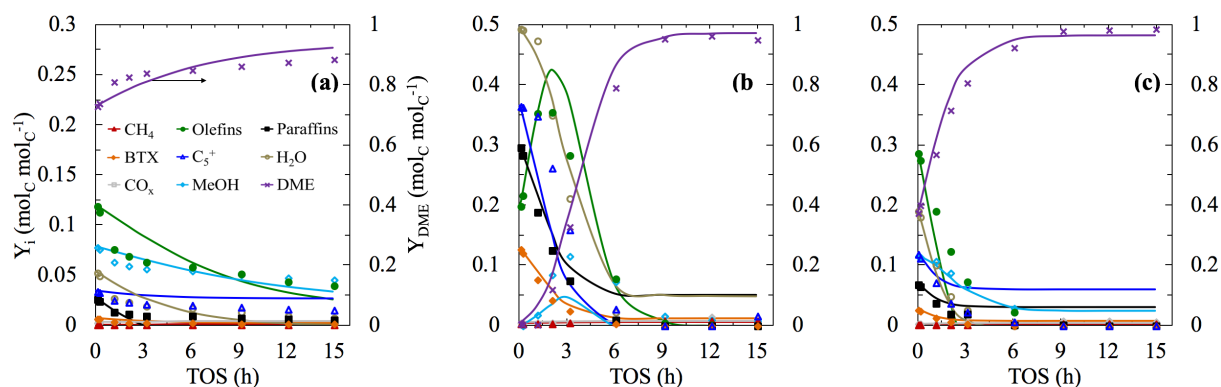

Figure 17. Comparison of the experimental data (dots) and those estimated with the kinetic model H (lines) for the evolution with time on stream of the product molar fractions for a pure DME feed at (a) 325 ºC and 2 g_{cat} h mol_C^{-1}, (b) 375 ºC and 2 g_{cat} h mol_C^{-1}, and (c) 375 ºC and 0.5 g_{cat} h mol_C^{-1}.

Model H fits zero-time kinetics with a similar quality model B does. It also undergoes similar difficulties for fitting TOS values when conditions are more extreme. However, the visual improvement model H provides with respect to model B is notorious for milder conditions (like TOS at 375 ºC and 2 g_{cat} h mol_C^{-1} or 325 ºC and 2 g_{cat} h molC^{-1}, in Figures 15a and 17a, and Figures 15c and 17c, respectively). Such enhancement in the quality of fitting at milder conditions for TOS is even more relevant at 350 ºC and 2 g_{cat} h mol_C^{-1}, as shown in Figure 18.
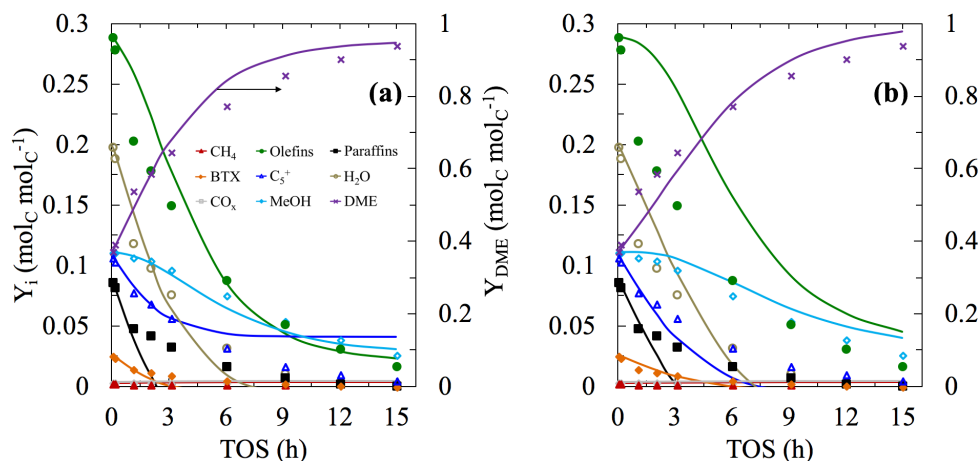
Figure 18. Comparison of the experimental data (dots) and those estimated with the kinetic model (lines) (a) B and (b) H for the evolution with time on stream of the product molar fractions for a pure DME feed at 350 ºC and 2 g_{cat} h mol_C^{-1}.

Yet the benefits model H brings are visually perceptible, how significant they are with respect to model B only their statistical analysis can reveal.

4.3.3. Discrimination of models with different number of deactivation kinetic constants

In order to identify which model (B or H) is more determining, models B and H were compared. Note that models with different number of degrees of freedom were compared (ν_B=783 and ν_H=781), hence Equation (28) applies. A 95% confidence interval was established. In Table 6 fundamental features for that discrimination are displayed.

Table 6. Statistical comparison of models with different number of kinetic constants.

Model	B	H
SSE	$3.21 \ 10^{-2}$	$3.08 \ 10^{-2}$
s^2	$2.29 \ 10^{-3}$	$2.26 \ 10^{-3}$
F	$17.14 \ (F_{B-H})$	
$F_{1-\alpha}$	3.01	

Their Fisher test reveals that the decrease in degrees of freedom in model H by increasing the number of kinetic constants involved provides a significant improvement with respect to model B, since the inequation (Eq. (28)) is by far satisfied (17.14>3.01). Such outcome is observed notwithstanding their akin variances, because when comparing models with different number of degrees of freedom (with Eq. (28)), the effect of the variance is limited with respect to that of the SSE.

Statistics-driven results are coherent with what previously stated, thereby confirming not only that model H is significantly better than model B, but also that DME undergoes a segregated pathway (thus forming coke at a different rate) with respect to the rest of the species.

4.4. KINETIC PARAMETERS

According to the previous section, model H best fits experimental data. The values of the kinetic parameters of best fit are shown in Table 7. These include, among others, the kinetic constants at a reference temperature, 350 °C, and activation energies for both the reactions defined in Figure 11 and the deactivation equation.

Table 7. Kinetic parameters proposed by model H for the DTO reaction considering catalyst deactivation and a pure DME feed.

Parameter	k^* / K^* (at 350 ºC)	E / ΔH (kJ mol^{-1})
Reaction scheme		
k_1 (mol$_C$ g$_{cat}^{-1}$ h^{-1} atm^{-2})	$4.98 \ 10^2$	$1.27 \ 10^1$
k_2 (mol$_C$ g$_{cat}^{-1}$ h^{-1} atm^{-1})	$2.34 \ 10^0$	$2.63 \ 10^1$
k_3 (mol$_C$ g$_{cat}^{-1}$ h^{-1} atm^{-1})	$3.24 \ 10^{-1}$	$3.59 \ 10^1$
k_4 (mol$_C$ g$_{cat}^{-1}$ h^{-1} atm^{-2})	$2.71 \ 10^1$	$5.24 \ 10^1$
k_5 (mol$_C$ g$_{cat}^{-1}$ h^{-1} atm^{-2})	$8.77 \ 10^0$	$1.81 \ 10^1$
k_6 (mol$_C$ g$_{cat}^{-1}$ h^{-1} atm^{-1})	$1.92 \ 10^1$	$6.45 \ 10^0$
k_7 (mol$_C$ g$_{cat}^{-1}$ h^{-1} atm^{-1})	$9.77 \ 10^0$	$4.10 \ 10^1$
k_8 (mol$_C$ g$_{cat}^{-1}$ h^{-1} atm^{-1})	$4.74 \ 10^0$	$2.68 \ 10^1$
k_9 (mol$_C$ g$_{cat}^{-1}$ h^{-1} atm^{-1})	$4.90 \ 10^{-1}$	$5.24 \ 10^{-1}$
k_{10} (mol$_C$ g$_{cat}^{-1}$ h^{-1} atm^{-1})	$2.35 \ 10^{-2}$	$1.82 \ 10^{-1}$
K_a (atm^{-1})	$2.28 \ 10^{-2}$	$2.09 \ 10^{-1}$
Deactivation equation		
k_1 (h^{-1} atm^{-1})	$2.19 \ 10^{-1}$	$1.59 \ 10^1$
k_2 (h^{-1} atm^{-1})	$5.09 \ 10^{-1}$	$1.49 \ 10^1$
$K_{W,d}$ (atm^{-1})	$2.74 \ 10^{-2}$	$4.93 \ 10^1$
d	$9.78 \ 10^{-1}$	

Kinetic parameters in Table 7 confirm many of the statements made though the entire work. Firstly, the value of the kinetic constant for the DME hydrolysis (k_1) is meaningfully higher than in any other reaction. Indeed, such constant is 18 times bigger than the second highest kinetic constant (k_4), the latter being the autocatalytic conversion of DME into olefins, a reaction considered to be reasonably quick on account of its nature. So, the assumption made about equilibrium between methanol and DME being nearly instantly reached is proved to be correct, apart from being consistent with what the literature predicates, where both are considered as a single reactant (Menges and Kraushaar-Czarnetzki, 2012).

When comparing reactions where the olefin lump is formed, it is to be highlighted that kinetic constants in autocatalytic reactions are prominently ahead of those which are not autocatalytic ($k_4>k_2$ and $k_5>k_3$). That is consistent with the physical meaning of an autocatalytic reaction when compared to a non-autocatalytic reaction.

Besides, apart from autocatalytic reactions being quicker, kinetic constants of reactions yielding olefins from DME are an order of magnitude bigger than those in which methanol is converted to olefins (that is to say, $k_2>k_3$ and $k_4>k_5$). Concerning the issue, Pérez-Uriarte et al. (2016a) present similar results, which they link to the great ability DME has for reacting with the methoxy groups forming propylene by means of an additional route to the dual cycle. That implies DME being more reactive than methanol, as Gayubo et al. (2004) suggested.

According to the values of the kinetic constants of secondary reactions (k_6, k_7, k_8), it is clear to say that they are of substantial importance within the reaction scheme, as their constants are similar to the one that the autocatalytic transformation of DME to olefins shows, in terms of orders of magnitude. Furthermore, when temperature is increased, the importance of hydrogen transfer and oligomerisation reaction grows faster with respect to the main reactions, as the values of their activation energy are higher. Accordingly, yields of C_5^+ aliphatics and paraffins are mostly benefitted when temperature is increased, in detriment of the olefin lump yield, thereby Figure 9b being self-explanatory. That is attributed to the high acidity of the catalyst employed.

Thermal cracking is kinetically unimportant as suggested before, showing a constant at reference temperature of several orders of magnitude (1-3) smaller than any other reaction studied so far; such is predictable when looking at CH_4 and CO_x yields in Figure 9a. In fact, it has been reported to grow in importance under considerable temperatures (>500 ºC) (Aguayo et al., 2010), so it is clear that operation temperatures employed are not considerable when it comes to thermal cracking.

Concerning deactivation parameters, the most remarkable feature is that the deactivation constant for the hydrocarbon products (k_{d2}) doubles the one multiplying DME partial pressure (k_{d1}). As a result, the pathway by which products form coke is quicker than the one DME follows, yet it cannot be stated that the former is of more importance because under certain conditions (low temperatures and space time), partial pressure of DME is overwhelmingly higher than the sum of the partial pressures of the products.

4.5. WATER CO-FEEDING

In this section how the chosen model H predicts the evolution of the reactions and fits them into the experimental data when water was co-fed is analysed. Handling feeds with water implies being able to fit the experimental data from both a pure DME feed and a feed containing DME + water simultaneously.

4.5.1. Experimental fitting

The fitting of model H for both a pure feed and water co-feeding is displayed in the subsequent Figures 19 and 20 at zero time and Figures 21 and 22 with the TOS.

Figure 19. Comparison of the experimental data (dots) and those estimated with the kinetic model H (lines) for the evolution with space time of the product molar fractions for a pure DME feed at zero time on stream and at (a) 325 ºC, (b) 350 ºC and (c) 375 ºC.
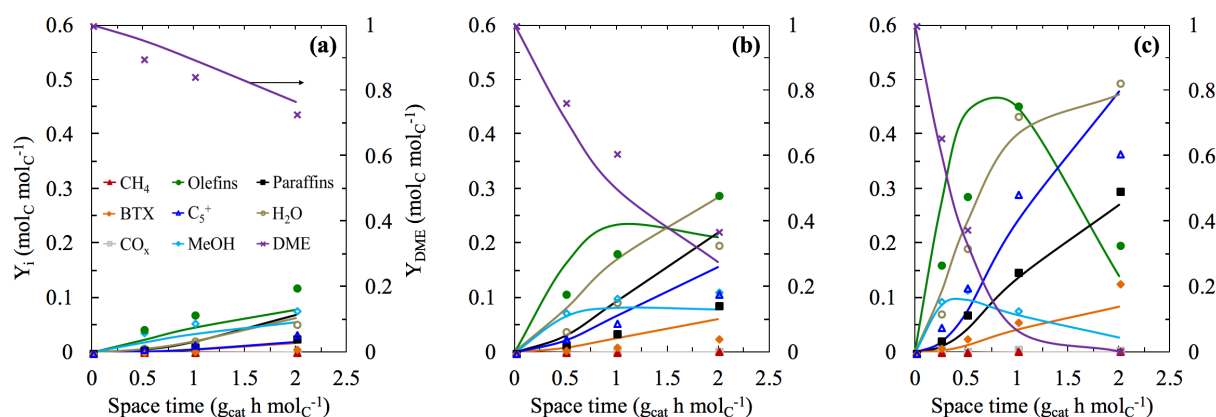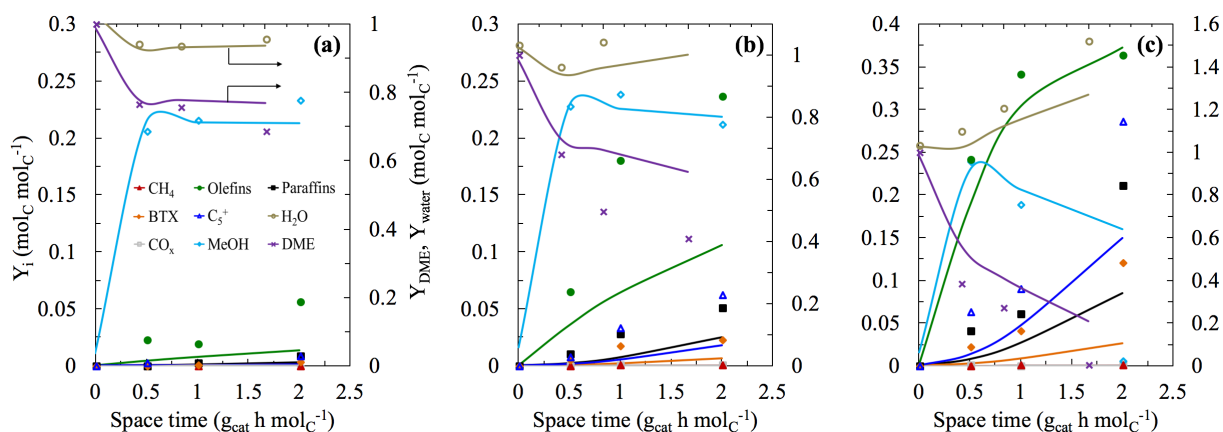
Figure 20. Comparison of the experimental data (dots) and those estimated with the kinetic model H (lines) for the evolution with space time of the product molar fractions for water co-feeding at zero time on stream and at (a) 325 ºC, (b) 350 ºC and (c) 375 ºC.

Figure 21. Comparison of the experimental data (dots) and those estimated with the kinetic model H (lines) for the evolution with time on stream of the product molar fractions for a pure DME feed at (a) 325 ºC and 2 g_{cat} h mol_C^{-1}, (b) 375 ºC and 2 g_{cat} h mol_C^{-1}, and (c) 375 ºC and 0.5 g_{cat} h mol_C^{-1}.
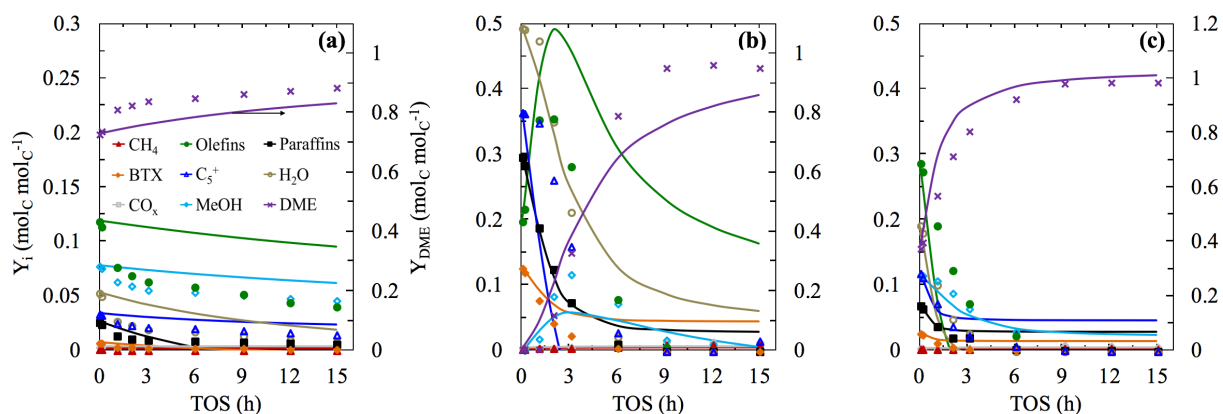

Figure 22. Comparison of the experimental data (dots) and those estimated with the kinetic model H (lines) for the evolution with time on stream of the product molar fractions for water co-feeding at (a) 325 ºC and 2 g_{cat} h mol_C^{-1}, (b) 375 ºC and 2 g_{cat} h mol_C^{-1}, and (c) 375 ºC and 0.5 g_{cat} h mol_C^{-1}.

On the one hand, Figure 19 and 20 reveal the quality of the fitting at zero-time model H is capable of providing, for both the DME feed (Figure 19) and when water is co-fed (Figure 20). Actually, it is remarkable that the fittings observed at zero time for the DME feed truly resemble those of Figures 16a, 16b and 16c, when water in the feed was not contemplated. Even more, the quality of the fitting Figures 20a, 20b and 20c depict (when water co-fed) are properly accurate, as, despite showing some flaws in the fitting of products coming from secondary reactions, the fitting of the main lumps involved in the medium (water, DME, methanol) is noteworthy.

On the other hand, Figure 21c reveals that when modelling deactivation for both feeds, same limitations observed in Figure 17c at extreme conditions exist. As it happened when a single kind of feed was analysed at high temperatures and low space times, deactivation takes place so rapidly that the model is only capable of fitting satisfactorily the evolution of DME over time. Still, as temperatures are decreased and/or space time increased, conditions are milder, favouring a slower and steadier deactivation which results in a better fitting. Let alone when water is co-fed, as portrayed in Figures 22a, 22b and 22c, where the quality of fitting is evident. It is true that by direct comparison with Figures 17a and 17b, Figures 21a and 21b show slightly worse performance, expected as they are part of a bigger group of experiments (hence higher number of degrees of freedom). Anyway, as to prove the capability of the model to deal with it, as an example another fitting is displayed in Figure 23.
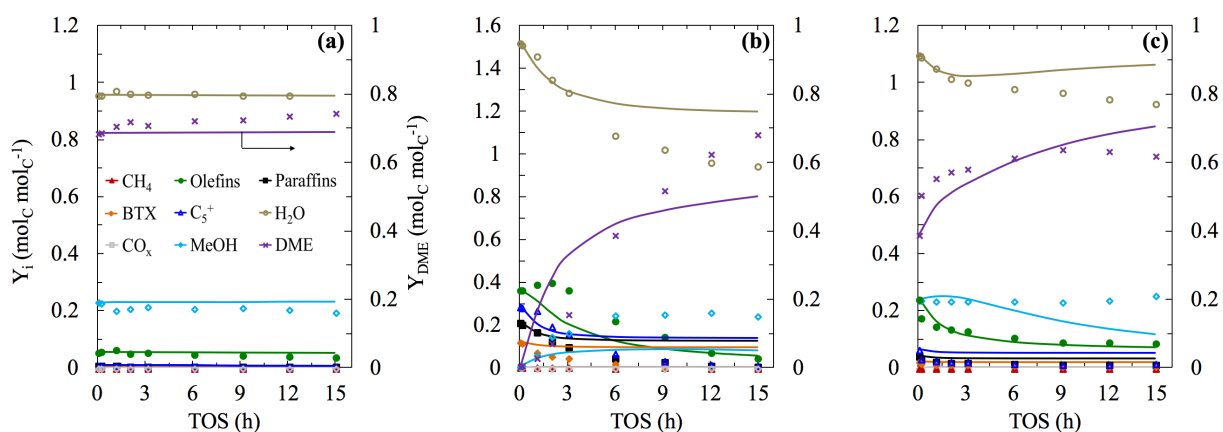

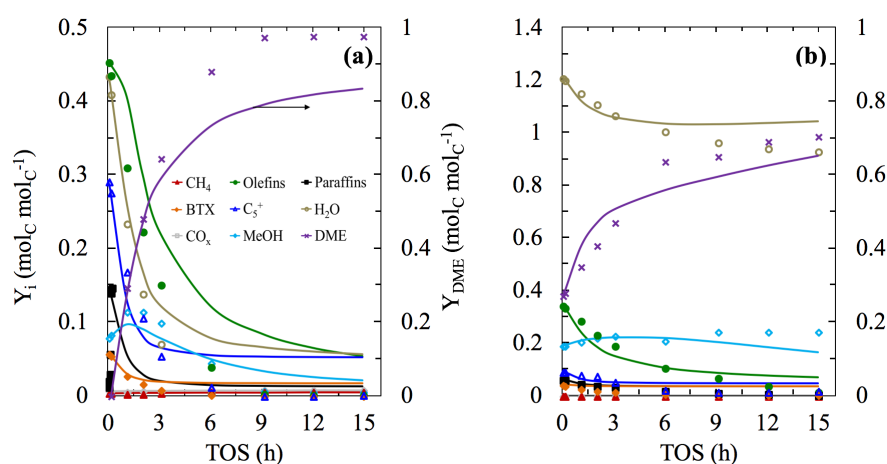**Figure 23**. Comparison of the experimental data (dots) and those estimated with the kinetic model H (lines) for the evolution with time on stream of the product molar fractions for (a) pure DME feed (b) water co-feeding at 375 ºC and 1 g_{cat} h mol_C^{-1}.

4.5.2. Kinetic parameters

In Table 8 the kinetic parameters corresponding to the simultaneous modelling of both feeds are displayed.

Table 8. Kinetic parameters proposed by model H for the DTO considering catalyst deactivation and the two kinds of feeds.

Parameter	k^* / K^* (at 350 ºC)		$E / \Delta H$ (kJ mol^{-1})
Reaction scheme			
k_1 (mol$_C$ g$_{cat}^{-1}$ h^{-1} atm^{-2})	$2.33\ 10^2$		$1.29\ 10^1$
k_2 (mol$_C$ g$_{cat}^{-1}$ h^{-1} atm^{-1})	$5.33\ 10^0$		$6.89\ 10^1$
k_3 (mol$_C$ g$_{cat}^{-1}$ h^{-1} atm^{-1})	$1.07\ 10^{-1}$		$3.61\ 10^1$
k_4 (mol$_C$ g$_{cat}^{-1}$ h^{-1} atm^{-2})	$4.03\ 10^1$		$1.49\ 10^1$
k_5 (mol$_C$ g$_{cat}^{-1}$ h^{-1} atm^{-2})	$2.25\ 10^1$		$1.82\ 10^1$
k_6 (mol$_C$ g$_{cat}^{-1}$ h^{-1} atm^{-1})	$3.51\ 10^1$		$6.63\ 10^{-1}$
k_7 (mol$_C$ g$_{cat}^{-1}$ h^{-1} atm^{-1})	$2.48\ 10^1$		$3.00\ 10^1$
k_8 (mol$_C$ g$_{cat}^{-1}$ h^{-1} atm^{-1})	$9.60\ 10^0$		$4.17\ 10^0$
k_9 (mol$_C$ g$_{cat}^{-1}$ h^{-1} atm^{-1})	$2.61\ 10^{-1}$		$5.18\ 10^{-1}$
k_{10} (mol$_C$ g$_{cat}^{-1}$ h^{-1} atm^{-1})	$1.10\ 10^{-2}$		$1.20\ 10^1$
K_a (atm^{-1})	$3.40\ 10^{-1}$		$1.06\ 10^{-1}$
Deactivation equation			
k_1 (h^{-1} atm^{-1})	$3.95\ 10^{-1}$		$8.09\ 10^1$
k_2 (h^{-1} atm^{-1})	$3.61\ 10^{-1}$		$6.68\ 10^0$
$K_{W,d}$ (atm^{-1})	$2.86\ 10^{-2}$		$5.10\ 10^1$
d		$2.09\ 10^0$	

It is to be mentioned that as in such figures fitting to experimental data for the two kind of feeds is done, the effect of water in the progress of the reactions and deactivation is reflected in values from Table 8, with respect to those in Table 7.

First of all, the change in the value of k_1 from Table 7 to Table 8 is noteworthy, as its value in the latter table drops to more than half of its value in Table 7 (from 498 to 233). That is very significant, since k_1 is closely related to the velocity of the thermodynamic equilibrium of DME and methanol. So, rate of DME hydrolysis is slowed as DME molecules compete with water to adsorb in the acid sites of the catalyst. As the reversibility of reaction step 1 in the kinetic scheme was defined with the equilibrium constant (which is only temperature dependant), it can be concluded that k-1 dropped as well to keep the k_1/k_{-1} ratio. Besides, it is evident that the value of k_1 is consistent with respect to the rest of steps as it is still an order of magnitude ahead of the kinetic constants corresponding to autocatalytic reactions.

Besides, kinetic constants for reactions in which olefins are formed (k_2, k_3, k_4 and k_5) in Table 8 keep their relationships shown in Table 7 intact. That means that reactions in which DME is involved present higher kinetic constant values ($k_2 > k_3$ and $k_4 > k_5$). Same pattern is observed for autocatalytic reactions, which present larger reaction rates than those reactions not self-catalysed ($k_4 > k_2$ and $k_5 > k_3$). It is needless to say that such relationships are expected to not be affected by water in the feed, for they ate inherent to the reaction nature and water in the feed does not alter the reaction itself.

Secondary reactions present increased values of kinetic constants (k_6, k_7 and k_8)) from Table 7 to Table 8, being their increase the highest. Given that in Figure 10a it is portrayed how the selectivity of the olefin lump benefits from water co-feeding in detriment of paraffins and aliphatics, values of k_6, k_7 and k_8 are not entirely consistent with those expected. Thereby, selectivity of the different lumps seems to be related by more than just the kinetic constants. On the other hand, the value of the kinetic constant for the DME thermal cracking reaction (k_{10}) says within the same range as when only the pure feed was considered, being consistent with

the idea that it is notoriously influenced by reaction temperature, which remained unchanged when considering water in the feed.

Concerning deactivation, the main change witnessed is the value of the order, which is doubled from one case to the other (from nearly 1 to 2). Such observation is coherent with water hindering deactivation, for increasing deactivation order results in a slower deactivation, in terms of mathematics. It is also noticeable that the deactivation constant for DME and the hydrocarbon products (k_{d1} and k_{d2}, respectively) present similar values when water in the feed is considered, as opposed when it is not ($k_{d1} < k_{d2}$). In other words, the greater the presence of water in the medium is, the quicker coke formation from DME is. If the fact that DME is more abundant is also mentioned as a consequence of the hindered conversions, it is concluded that water in the feed fosters in-parallel deactivation.

4.6. FUTURE WORK

The present contribution exposes two main potential recommended areas:

1. Polishing the proposed kinetic model. It was shown to respectably fit the experimental data, but there is still room for improvement. Using selective deactivation models, where more than one activities are involved, seems to be a promising idea. In principle, such models are able of providing a more flexible fitting to the experimental data. Still, these models also entail overparametrisation (which strongly depends on how many new parameters are added) and a very poor understanding (as implies that a single catalyst has several activities). Thereby, a two-activity deactivation model is considered to be a plausible alternative, where each of the activities is related to the strong and weak acidic sites present in the catalyst, respectively.

2. Confirming the reproducibility of the results obtained. In order to see how trustful obtained results are, simulating the experiments arises as a valid option. It is known that specific software for simulating multiphysics exists, which allows performing simulations based of strict thermodynamics in a CAD based reactor. As a result, 3D concentration, velocity and temperature profiles are obtained, which ease the visualisation of the effect of variables such as water, reaction temperature or space time.

5. CONCLUSIONS

- It was evidenced that the catalyst used, a very acid HZSM-5 (Si/Al=15), is suitable for DTO concerns. It was seen that by means of its remarkable stability, it maximised light olefin conversion without renouncing a strong resistance to deactivation, even at high TOS values. These results are consistent with the reported studies for the same catalyst with a more moderate acidity.

- Co-feeding water, despite causing a drop of conversion, showed promising results for its role in hindering deactivation. In such way, one of the advantage MTO has over DTO is dealt. It also affected product distribution since an increase in olefin selectivity in disfavour of secondary paraffins and aliphatics was witnessed.

- The behaviour of the compounds existent in the reaction when DME fed was predicted by lump-based kinetic models, each one comprising 9 lumps, a reaction scheme of 10 steps and a deactivation equation. 8 different deactivation equations were studied according to the lumps responsible for the deactivation.

- Out of all the models comprising different deactivation equations suggested, model H showed to fit most closely to experimental data, according to a statistics-driven discrimination procedure. Model H involves a DME and hydrocarbon-based coke formation deactivation, which happen through different rates as their distinctive kinetic constants reveal. This two kinetic constant model was found to be plausible although complete in-series and in-parallel mechanism were discarded on account of their lack of significance. Besides, for the same reason, methanol was also rejected from being a coking agent.

- Not only was chosen model H able to predict lump behaviour in the reactor for a pure DME feed, but it also proved to be valid at simultaneously fitting experimental data in water co-feeding cases. Water co-feeding is a common resource in the MTO industry for the reasons aforementioned. Therefore, the versatility of model H regarding this issue places it in a promising location for industrial implementation of the analogous.

6. NOMENCLATURE

a	Activity parameter
A	Extraframework cation
d	Deactivation order
D_e	Effective dispersion coefficient, $m^2\ h^{-1}$
d_p	Particle diameter, mm
E, E_j, E_d	Activation energy term, activation energy of reaction step j and activation energy of deactivation reactions, respectively, $kJ\ mol^{-1}$
F	Fisher distribution
F_C	Total carbon molar flow rate, $mol_C\ h^{-1}$
F_T	Total molar flow rate, $mol\ h^{-1}$
k, k^*	Kinetic constant and the corresponding term at the reference temperature
k_d, k_d^*	Deactivation kinetic constant and the corresponding value at the reference temperature, respectively, $h^{-1}atm^{-1}$
k_j, k_j^*	Kinetic constant of reaction step j, and the corresponding value at the reference temperature, respectively, $mol_C\ g_{cat}^{-1}\ h^{-1}\ atm^{-2}$ for a single reacting lump and $mol_C\ g_{cat}^{-1}\ h^{-1}\ atm^{-2}$ for two reacting lumps
K	Equilibrium constant for the DME hydrolysis reaction, dimensionless
K_a, K_a^*	Parameter quantifying the adsorption of both methanol and water, and the corresponding value at the reference temperature, respectively, atm^{-1}
$K_{W,d}, K_{W,d}^*$	Parameter quantifying the adsorption of water, and the corresponding value at the reference temperature, respectively, atm^{-1}
l	Reactor bed length, m
m	Charge of the extraframework cation
N_C	Ratio of carbon molar flow rate to total mass flow rate, $mol_C\ mol^{-1}$
$n_{e,0}, n_{e,d}$	Number of experiments at zero and at t time on stream, respectively
n_l, n_p	Number of lumps and parameters of the model, respectively
n_R	Reaction order of the R lumps present in reaction step j
P	Total pressure, atm
P_{cp}, P_M, P_W	Partial pressure of the coke precursors, methanol and water, respectively, atm
P_R	Partial pressure of the R lumps present in step j, atm
R	Universal gas constant
r_d	Deactivation rate, h^{-1}
r_i	Formation rate of lump i, $mol_C\ h^{-1}\ g_{cat}^{-1}$
r_j	Reaction rate of reaction step j, $mol_C\ h^{-1}\ g_{cat}^{-1}$
$r_{j,0}$	Reaction rate of reaction step j at zero time, $mol_C\ h^{-1}\ g_{cat}^{-1}$
R_n	Number of runs repeated at the same conditions
S	Reactor section, m^2
S_i	Selectivity of lump i, expressed in carbon units ($mol_C\ mol_C^{-1}$)
s^2	Variance of the lack of fit
S_{BET}, S_{mes}	BET and external surface area, respectively, $m^2\ g^{-1}$
SSE	Sum of the square errors

T, T*	Temperature and reference temperature, respectively, ºC
t	Time, h
TOS	Time on stream, h
v	Bulk velocity, m/s
$(v_i)_j$	Carbon balance coefficient of each i lump in the j reaction step, dimensionless
$V_{mesopore}, V_{micropore}$	Mesopore and micropore volume, respectively, $cm^3 \, g^{-1}$
W	Catalyst mass, g
X	Conversion of methanol and DME, expressed in carbon units ($mol_C \, mol_C^{-1}$)
x/y	Proportion of Si and Al in the structure, Si/Al ratio, dimensionless
x+y	Number of tetrahedra per crystallographic unit
Y_i	Yield of lump i, expressed in carbon units ($mol_C \, mol_C^{-1}$)
y_i	Lump i molar fraction, expressed in carbo units ($mol_C \, mol_C^{-1}$)
$y_{i,0}, y_{i,in}$	Molar fraction of lump i at zero-time on stream and at the inlet of the reactor, respectively, expressed in carbon units ($mol_C \, mol_C^{-1}$)
$y_{i,n}^0, y_{i,n}^t$	Calculated molar fraction of lump i at n experimental condition at zero and at t time on stream, respectively, expressed in carbon units ($mol_C \, mol_C^{-1}$)
$y_{i,n}^{0*}, y_{i,n}^{t*}$	Experimental molar fraction of lump i at n experimental condition at zero and at t time on stream, respectively, expressed in carbon units ($mol_C \, mol_C^{-1}$)
z	Number of water molecules per extraframework cation

6.1. GREEK LETTERS AND SYMBOLS

α	Confidence level
ΔH_a	Apparent adsorption heat of methanol and water, kJ mol^{-1}
$\Delta H_{W,d}$	Apparent adsorption heat of water, kJ mol^{-1}
ε_b	Effective bed-particle porosity
μ-GC	Micro gas chromatograph
ν	Degrees of freedom of the model
θ	Factor representing reaction attenuation by adsorption of water and methanol in catalyst acidic sites
θ_d	Factor representing deactivation attenuation by adsorption of water catalyst acidic sites
ρ_b	Bed density, kg m^{-3}
τ	Space time, g_{cat} h mol_C^{-1}

6.2. ACHRONYMS AND ABBREVIATIONS

BET	Brunauer-Emmet-Teller
CDA	Catalytic dehydrogenation of alkanes
DME	Dimethyl ether
DTO	Dimethyl ether to olefins
FCC	Fluid catalytic cracking
FTS	Fischer-Tropsch synthesis
HCP	Hydrocarbon pool

HZSM	Protonated form of the ZSM
MMt	Millions of metric tons
MTG	Methanol to gasoline
MTH	Methanol to hydrocarbons
MTO	Methanol to olefins
MTP	Methanol to propylene
OCM	Oxidative coupling of methane
OCP	Olefin cracking process
ODE	Ordinary differential equation
SAPOs	Silicoaluminophosphates
SC	Steam cracking
STD	Syngas to dimethyl ether
STM	Syngas to methanol
t-BA	Tert-butylamine
TPD	Temperature programmed desorption

6.3. ABBREVIATIONS OF LUMPS

D	Dimethyl ether
M	Methanol
W	Water
O	C_2-C_4 ranged olefins
P	C_2-C_4 ranged paraffins
C_5^+	C_5^+ aliphatics
BTX	Aromatics (Benzene, Toluene, Xylene)
CO_x	CO and CO_2
CH_4	Methane

7. REFERENCES

Aguayo, A.T., Ereña, J., Mier, D., Arandes, J.M., Olazar, M., Bilbao, J., 2007. Kinetic modeling of dimethyl ether synthesis in a single step on a CuO-ZnO-Al$_2$O$_3$/γ-Al$_2$O$_3$ catalyst. Ind. Eng. Chem. Res. 46, 5522–5530.

Aguayo, A.T., Gayubo, A.G., Vivanco, R., Olazar, M., Bilbao, J., 2005. Role of acidity and microporous structure in alternative catalysts for the transformation of methanol into olefins. Appl. Catal. A Gen. 283, 197–207.

Aguayo, A.T., Mier, D., Gayubo, A.G., Bilbao, J., 2010. Kinetics of Methanol Transformation into Hydrocarbons on a HZSM-5 Zeolite Catalyst at High Temperature (400-550 °C). Ind. Eng. Chem. Res. 12371–12378.

Al-Dughaither, A.S., De Lasa, H., 2014. Neat dimethyl ether conversion to olefins (DTO) over HZSM-5: Effect of SiO2/Al2O3on porosity, surface chemistry, and reactivity. Fuel 138, 52–64.

Amghizar, I., Vandewalle, L.A., Van Geem, K.M., Marin, G.B., 2017. New Trends in Olefin Production. Engineering 3, 171–178.

Arstad, B., Kolboe, S., 2001. The reactivity of molecules trapped within the SAPO-34 cavities in the methanol-to-hydrocarbons reaction. J. Am. Chem. Soc. 123, 8137–8138.

Becker, P.J., Serrand, N., Celse, B., Guillaume, D., Dulot, H., 2016. Comparing hydrocracking models: Continuous lumping vs. single events. Fuel 165, 306–315.

Biryukova, E.N., Goryainova, T.I., Kulumbegov, R. V., Kolesnichenko, N. V., Khadzhiev, S.N., 2011. Conversion of dimethyl ether into lower olefins on a La-Zr-HZSM-5/Al$_2$O$_3$ zeolite catalyst. Pet. Chem. 51, 49–54.

Bjørgen, M., Joensen, F., Lillerud, K.P., Olsbye, U., Svelle, S., 2009. The mechanisms of ethene and propene formation from methanol over high silica H-ZSM-5 and H-beta. Catal. Today 142, 90–97.

Bjørgen, M., Svelle, S., Joensen, F., Nerlov, J., Kolboe, S., Bonino, F., Palumbo, L., Bordiga, S., Olsbye, U., 2007. Conversion of methanol to hydrocarbons over zeolite H-ZSM-5: On the origin of the olefinic species. J. Catal. 249, 195–207.

Bleken, F.L., Skistad, W., Barbera, K., Kustova, M., Bordiga, S., Beato, P., Lillerud, K.P., Svelle, S., Olsbye, U., 2011. Conversion of methanol over 10-ring zeolites with differing volumes at channel intersections: comparison of TNU-9, IM-5, ZSM-11 and ZSM-5. Phys. Chem. Chem. Phys. 13, 2539–2549.

Cai, G., Liu, Z., Shi, R., Changqing, H., Yang, L., Sun, C., Chang, Y., 1995. Light alkenes from syngas via dimethyl ether. Appl. Catal. A, Gen. 125, 29–38.

Chapra, S.C., Canale, R.P., 2010. Multidimensional unconstrained optimization, in: Numerical Methods for Engineers, 6th ed. McGraw-Hill, New York, pp. 372-374.

Cheetham, A.K., Férey, G., Loiseau, T., 1999. Open-Framework Inorganic Materials. Angew. Chemie Int. Ed. 38, 3268–3292.

Chen, D., Moljord, K., Fuglerud, T., Holmen, A., 1999. The effect of crystal size of SAPO-34 on the selectivity and deactivation of the MTO reaction. Microporous Mesoporous Mater. 29, 191–203.

Chen, J., Wright, P.A., Natarajan, S., Thomas, J.M., 1994. Understanding The Brønsted Acidity of SAPO-5, SAPO-17, SAPO-18 and SAPO-34 and Their Catalytic Performance for Methanol Conversion to Hydrocarbons. Stud. Surf. Sci. Catal. 84, 1731–1738.

Chen, N.Y., Reagan, W.J., 1979. Evidence of autocatalysis in methanol to hydrocarbon reactions over zeolite catalysts. J. Catal. 59, 123–129.

Christensen, G., Apelian, M.R., Hickey, K.J., Jaffe, S.B., 1999. Future directions in modeling the FCC process: An emphasis on product quality. Chem. Eng. Sci. 54, 2753–2764.

Cordero-Lanzac, T., Aguayo, A.T., Gayubo, A.G., Castaño, P., Bilbao, J., 2018. Simultaneous modeling of the kinetics for n-pentane cracking and the deactivation of a HZSM-5 based catalyst. Chem. Eng. J. 331, 818–830.

Dahl, I.M., Kolboe, S., 1993. On the reaction mechanism for propene formation in the MTO reaction over SAPO-34. Catal. Letters 20, 329–336.

Derouane, E.G., Dejaifve, P., Gabelica, Z., Védrine, J.C., 1981. Molecular shape selectivity of ZSM-5, modified ZSM-5 and ZSM-11 type zeolites. Faraday Discuss. Chem. Soc. 72, 331.

Dessau, R.M., LaPierre, R.B., 1982. On the mechanism of methanol conversion to hydrocarbons over HZSM-5. J. Catal. 78, 136–141.

De Oliveira, L.P., Hudebine, D., Guillaume, D., Verstraete, J.J., 2016. A Review of Kinetic Modeling Methodologies for Complex Processes. Oil Gas Sci. Technol. 71., 1-50.

Flanigen, E.M., 2001. Chapter 2: Zeolites and Molecular Sieves an Historical Perspective, in: van Bekkum, H., Flanigen, E.M., Jacobs, P.A., Jansen, J.C., 2001. Introduction to zeolite science and practice 137, 2nd ed. Elsevier Science, Amsterdam, pp. 11-35.

Froment, G.F., 2005. Single Event Kinetic Modeling of Complex Catalytic Processes. Catal. Rev. 47, 83–124.

Funk, G.A., Myers, D., Vora, B., 2013. A different game plan. Hydrocarb. Eng. 1–4.

Gayubo, A.G., Aguayo, A.T., Castilla, M., Morán, A.L., Bilbao, J., 2004. Role of water in the kinetic modeling of methanol transformation into hydrocarbons on HZSM-5 zeolite. Chem. Eng. Commun. 191, 944–967.

Gayubo, A.G., Aguayo, A.T., Olazar, M., Vivanco, R., Bilbao, J., 2003. Kinetics of the irreversible deactivation of the HZSM-5 catalyst in the MTO process. Chem. Eng. Sci. 58, 5239–5249.

Ghavipour, M., Behbahani, R.M., Moradi, G.R., Soleimanimehr, A., 2013. Methanol dehydration over alkali-modified H-ZSM-5; Effect of temperature and water dilution on products distribution. Fuel 113, 310–317.

Guisnet, M., Costa, L., Ribeiro, F.R., 2009. Prevention of zeolite deactivation by coking. J. Mol. Catal. A Chem. 305, 69–83.

Harrison, I.D., Leach, H.F., Whan, D.A., 1987. Comparison of the shape selective properties of ferrierite, ZSM-5 and ZSM-11. Zeolites 7, 21–27.

Hyde, B., 2012. Light Olefins Market Review. PEMEX Petroquímica Forum. 2012.

Ilias, S., Bhan, A., 2013. Mechanism of the catalytic conversion of methanol to hydrocarbons. ACS Catal. 3, 18–31.

Jha, B., Singh, D.N., 2016. Chapter 2: Basics of zeolites, in: Fly Ash Zeolites, 1st ed. Springer, Singapore. pp. 5–31.

Jiang, S., Hwang, J.S., Jin, T., Cai, T., Cho, W., Baek, Y.S., Park, S.E., 2004. Dehydration of Methanol to Dimethyl Ether over ZSM-5 Zeolite. Bull. Korean Chem. Soc. 25, 185–189.

Keil, F.J., 1999. Methanol-to-hydrocarbons: process technology. Microporous Mesoporous Mater. 29, 49–66.

Khanmohammadi, M., Amani, S., Bagheri Garmarudi, A., Niaei, A., 2016. Methanol-to-propylene process: Perspective of the most important catalysts and their behavior. Cuihua Xuebao/Chinese J. Catal. 37, 325–339.

Lesthaeghe, D., Van Speybroeck, V., Marin, G.B., Waroquier, M., 2006. Understanding the failure of direct C-C coupling in the zeolite-catalyzed methanol-to-olefin process. Angew. Chemie - Int. Ed. 45, 1714–1719.

Lluch Urpí, J., 2011. Procesos y Esquemas de Refino, in: Tecnología y margen de refino del petróleo, 1st ed. Ediciones Díaz de Santos, Madrid. pp. 383-387.

Loewenstein, W., 1954. The distribution of aluminum in the tetrahedra of silicates and aluminates. Am. Mineral. 39, 92–96.

Luo, L., Tang, X., Wang, W., Wang, Y., Sun, S., Qi, F., Huang, W., 2013. Methyl radicals in oxidative coupling of methane directly confirmed by synchrotron VUV photoionization mass spectroscopy. Sci. Rep. 3, 1–7.

Marquardt, D., 1963. An Algorithm for Least-Squares Estimation of Nonlinear Parameters. BSIAM J. Appl. Math. 11, 431–441.

Menges, M., Kraushaar-Czarnetzki, B., 2012. Kinetics of methanol to olefins over AlPO4-bound ZSM-5 extrudates in a two-stage unit with dimethyl ether pre-reactor. Microporous Mesoporous Mater. 164, 172–181.

Mier, D., Aguayo, A.T., Gamero, M., Gayubo, A.G., Bilbao, J., 2010. Kinetic Modeling of n - Butane Cracking on HZSM-5 Zeolite Catalyst. Ind. Eng. Chem. Res. 49, 8415–8423.

Mikkelsen, Ø., Rønning, P.O., Kolboe, S., 2000. Use of isotopic labeling for mechanistic studies of the methanol-to-hydrocarbons reaction. Methylation of toluene with methanol over H-ZSM-5, H-mordenite and H-beta. Microporous Mesoporous Mater. 40, 95–113.

Müller, S., Liu, Y., Vishnuvarthan, M., Sun, X., Van Veen, A.C., Haller, G.L., Sanchez-Sanchez, M., Lercher, J.A., 2015. Coke formation and deactivation pathways on H-ZSM-5 in the conversion of methanol to olefins. J. Catal. 325, 48–59.

Olivos-Suarez, A.I., Szécsényi, À., Hensen, E.J.M., Ruiz-Martínez, J., Pidko, E.A., Gascon, J., 2016. Strategies for the Direct Catalytic Valorization of Methane Using Heterogeneous Catalysis: Challenges and Opportunities. ACS Catal. 6, 2965–2981.

Payra, P., Dutta, P.K., 2003. Zeolites: A Primer, in: Auerbach, S.M., Carrado, K.A., Dutta, P.K., 2003. Handbook of zeolite science and technology, 1st ed. Marcel Dekker, New York. pp. 1–19.

Pérez-Uriarte, P., Ateka, A., Aguayo, A.T., Gayubo, A.G., Bilbao, J., 2016a. Kinetic model for the reaction of DME to olefins over a HZSM-5 zeolite catalyst. Chem. Eng. J. 302, 801–810.

Pérez-Uriarte, P., Ateka, A., Gayubo, A.G., Cordero-Lanzac, T., Aguayo, A.T., Bilbao, J., 2017. Deactivation kinetics for the conversion of dimethyl ether to olefins over a HZSM-5 zeolite catalyst. Chem. Eng. J. 311, 367–377.

Pérez-Uriarte, P., Gamero, M., Ateka, A., Díaz, M., Aguayo, A.T., Bilbao, J., 2016b. Effect of the Acidity of HZSM-5 Zeolite and the Binder in the DME Transformation to Olefins. Ind. Eng. Chem. Res. 55, 1513–1521.

Pitault, I., Nevicato, D., Forissier, M., Bernard, J.R., 1994. Kinetic model based on a molecular description for catalytic cracking of vacuum gas oil. Chem. Eng. Sci. 49, 4249–4262.

Ren, T., Patel, M., Blok, K., 2006. Olefins from conventional and heavy feedstocks: Energy use in steam cracking and alternative processes. Energy 31, 425–451.

Sabbe, M.K., Van Geem, K.M., Reyniers, M.F., Marin, G.B., 2011. First principle-based simulation of ethane steam cracking. AIChE J. 57, 482–496.

Sardesai, A., Lee, S., 1998. Hydrocarbon synthesis from dimethyl ether over ZSM-5 catalyst. ACS Div. Fuel Chem. Prepr. 43, 722–724.

Sattler, J.J.H.B., Ruiz-Martínez, J., Santillan-Jimenez, E., Weckhuysen, B.M., 2014. Catalytic dehydrogenation of light alkanes on metals and metal oxides. Chem. Rev. 114, 10613–10653.

Schulz, H., 1999. Short history and present trends of Fischer–Tropsch synthesis. Appl. Catal. A Gen. 186, 3–12.

Seader, J.D., Henley, E.J., Roper, D.K., 2011. Chapter 3: Mass transfer in diffusion, in: Separation process principles: chemical and biochemical operations, 3rd ed. John Wiley & Sons, New York. pp. 107-114.

Sierra, I., Ereña, J., Aguayo, A.T., Ateka, A., Bilbao, J., 2013. Kinetic Modelling for the Dehydration of Methanol to Dimethyl Ether over γ-Al$_2$O$_3$. Chem. Eng. Trans. 32, 613–618.

Song, W., Marcus, D.M., Fu, H., Ehresmann, J.O., Haw, J.F., 2002. An oft-studied reaction that may never have been: Direct catalytic conversion of methanol or dimethyl ether to hydrocarbons on the solid acids HZSM-5 or HSAPO-34. J. Am. Chem. Soc. 124, 3844–3845.

Stöcker, M., 1999. Methanol-to-hydrocarbons: catalytic materials and their behavior. Microporous Mesoporous Mater. 29, 3–48.

Sun, X., Müller, S., Liu, Y., Shi, H., Haller, G.L., Sanchez-Sanchez, M., Van Veen, A.C., Lercher, J.A., 2014. On reaction pathways in the conversion of methanol to hydrocarbons on HZSM-5. J. Catal. 317, 185–197.

Svelle, S., Joensen, F., Nerlov, J., Olsbye, U., Lillerud, K.P., Kolboe, S., Bjørgen, M., 2006. Conversion of methanol into hydrocarbons over zeolite H-ZSM-5: Ethene formation is mechanistically separated from the formation of higher alkenes. J. Am. Chem. Soc. 128, 14770–14771.

Svelle, S., Olsbye, U., Joensen, F., Bjørgen, M., 2007. Conversion of methanol to alkenes over medium- and large-pore acidic zeolites: Steric manipulation of the reaction intermediates governs the ethene/propene product selectivity. J. Phys. Chem. C 111, 17981–17984.

Tau, L.M., Fort, A.W., Bao, S., Davis, B.H., 1990. Methanol to gasoline:14C tracer studies of the conversion of methanol/higher alcohol mixtures over ZSM-5. Fuel Process. Technol. 26, 209–219.

Teketel, S., Olsbye, U., Lillerud, K.P., Beato, P., Svelle, S., 2010. Selectivity control through fundamental mechanistic insight in the conversion of methanol to hydrocarbons over zeolites. Microporous Mesoporous Mater. 136, 33–41.

Tian, P., Wei, Y., Ye, M., Liu, Z., 2015. Methanol to olefins (MTO): From fundamentals to commercialization. ACS Catal. 5, 1922–1938.

Toch, K., Thybaut, J.W., Marin, G.B., 2015. A systematic methodology for kinetic modeling of chemical reactions applied to n-hexane hydroisomerization. AIChE J. 61, 880–892.

Wang, C., Xu, J., Qi, G., Gong, Y., Wang, W., Gao, P., Wang, Q., Feng, N., Liu, X., Deng, F., 2015. Methylbenzene hydrocarbon pool in methanol-to-olefins conversion over zeolite H-ZSM-5. J. Catal. 332, 127–137.

Wang, W., Buchholz, A., Seiler, M., Hunger, M., 2003. Evidence for an Initiation of the Methanol-to-Olefin Process by Reactive Surface Methoxy Groups on Acidic Zeolite Catalysts. J. Am. Chem. Soc. 125, 15260–15267.

Weekman, V.W., Nace, D.M., 1970. Kinetics of catalytic cracking selectivity in fixed, moving, and fluid bed reactors. AIChE J. 16, 397–404.

Weissermel, K., Arpe, H.-J., 1981. 3. Olefinas, in: Química orgánica industrial, 2nd ed. Reverté, Barcelona. pp 59-63.

Weitkamp, J., 2000. Zeolites and Catalysis. Solid State Ionics 131, 175–188.

Wendelbo, R., Akporiaye, D., Andersen, A., Dahl, I.M., Mostad, H.B., 1996. Synthesis, characterization and catalytic testing of SAPO-18, MgAPO-18, and ZnAPO-18 in the MTO reaction. Appl. Catal. A Gen. 142, 197–207.

Ying, L., Yuan, X., Ye, M., Cheng, Y., Li, X., Liu, Z., 2015. A seven lumped kinetic model for industrial catalyst in DMTO process. Chem. Eng. Res. Des. 100, 179–191.

Zimmermann, H., 2013. Propene. Ullmann's Encycl. Ind. Chem. 2013.

Zimmermann, H., Walzl, R., 2012. Ethene. Ullmann's Encycl. Ind. Chem. 2012.